

**This is the accepted manuscript version of the contribution published as:**

Laso-Pérez, R., Wegener, G., Knittel, K., Widdel, F., Harding, K.J., Krukenberg, V., Meier, D.V., **Richter, M.**, Tegetmeyer, H.E., Riedel, D., **Richnow, H.-H.**, **Adrian, L.**, **Reemtsma, T.**, **Lechtenfeld, O.J.**, **Musat, F.** (2016):

Thermophilic archaea activate butane via alkyl-coenzyme M formation  
*Nature* **539** (7629), 396 - 401

**The publisher's version is available at:**

<http://dx.doi.org/10.1038/nature20152>

## ARTICLE

doi:10.1038/nature20152

**Thermophilic archaea activate butane via alkyl-coenzyme M formation**

Rafael Laso-Pérez, Gunter Wegener, Katrin Knittel, Friedrich Widdel, Katie J. Harding, Viola Krukenberg, Dimitri V. Meier, Michael Richter, Halina E. Tegetmeyer, Dietmar Riedel, Hans-Hermann Richnow, Lorenz Adrian, Thorsten Reemtsma, Oliver Lechtenfeld & Florin Musat

This is a PDF file of a peer-reviewed paper that has been accepted for publication. Although unedited, the content has been subjected to preliminary formatting. *Nature* is providing this early version of the typeset paper as a service to our customers. The text and figures will undergo copyediting and a proof review before the paper is published in its final form. Please note that during the production process errors may be discovered which could affect the content, and all legal disclaimers apply.

Cite this article as: Laso-Pérez, R. *et al.* Thermophilic archaea activate butane via alkyl-coenzyme M formation. *Nature* <http://dx.doi.org/10.1038/nature20152> (2016).

Received 6 June; accepted 11 October 2016.

Accelerated Article Preview Published online 17 October 2016.

# Thermophilic archaea activate butane via alkyl-coenzyme M formation

Rafael Laso-Pérez<sup>1,2</sup>, Gunter Wegener<sup>1,2,3</sup>, Katrin Knittel<sup>1</sup>, Friedrich Widdel<sup>1</sup>, Katie J. Harding<sup>1§</sup>, Viola Krukenberg<sup>1,2</sup>, Dimitri V. Meier<sup>1</sup>, Michael Richter<sup>1</sup>, Halina E. Tegetmeyer<sup>2,4</sup>, Dietmar Riedel<sup>5</sup>, Hans-Hermann Richnow<sup>6</sup>, Lorenz Adrian<sup>6</sup>, Thorsten Reemtsma<sup>6</sup>, Oliver Lechtenfeld<sup>6</sup> & Florin Musat<sup>1,6</sup>

The anaerobic formation and oxidation of methane involve unique enzymatic mechanisms and cofactors that are believed to be all specific for C<sub>1</sub>-compounds. Here we found that an anaerobic thermophilic enrichment culture composed of dense consortia of archaea and bacteria apparently uses partly similar pathways to oxidize the C<sub>4</sub>-hydrocarbon butane. The archaea, proposed genus *Candidatus Syntrophoarchaeum*, showed the characteristic autofluorescence of methanogens, and contained highly expressed genes encoding enzymes similar to methyl-coenzyme M reductase (MCR). We detected butyl-coenzyme M, indicating archaeal butane activation in analogy to the first step in anaerobic methane oxidation. In addition, *Ca. Syntrophoarchaeum* expressed the genes encoding beta-oxidation enzymes, carbon monoxide dehydrogenase and reversible C<sub>1</sub>-methanogenesis enzymes. This allows complete oxidation of butane. Reducing equivalents are apparently channelled to HotSeep-1, a thermophilic sulfate-reducing partner bacterium known from the anaerobic oxidation of methane. Genes encoding 16S rRNA and MCR similar to those identifying *Ca. Syntrophoarchaeum* were repeatedly retrieved from marine subsurface sediments suggesting that the presented activation mechanism is naturally widespread in the anaerobic oxidation of short-chain hydrocarbons.

**Etymology.** *Syntrophoarchaeum*. *syn* (greek): together, *tropho* (greek) meaning nourishment, *archaeum* (greek): ancient; butanivorans, *butanum* (latin): butane, *vorans* (latin): eating, devouring. The name implies an organism capable of butane oxidation, however demanding syntrophic electron sinks. A second strain is named *Ca. S. caldarius*, *caldarius* (latin): warm/ hot, refers to its thermophilic growth condition. **Locality.** Enriched from hydrothermally-heated, hydrocarbon-rich marine sediments of the Guaymas Basin at 2000 m water depth, Gulf of California, Mexico.

**Diagnosis.** Anaerobic, butane-oxidizing archaeon, variable morphology, 1.5 × 1 µm, dependent on syntrophic support by the sulfate-reducing partner bacterium *Candidatus Desulfofervidus auxilii*.

Massive amounts of natural gas migrate from deep-seated reservoirs towards the seafloor<sup>1–3</sup>. Most of this gas is already consumed in the anoxic zone by microorganisms coupling oxidation of the hydrocarbons to the reduction of the abundant electron acceptor, sulfate. Research on the anaerobic oxidation of natural gas has been largely focused on methane as the most abundant constituent<sup>2–4</sup>. The anaerobic oxidation of methane (AOM) is carried out by anaerobic methanotrophic archaea (ANME) forming consortia with sulfate-reducing bacteria (SRB); ANME activate methane to methyl-coenzyme M by methyl-CoM reductases (MCR)<sup>4,5</sup>. The CoM-bound methyl group is further oxidized to CO<sub>2</sub> by reversing the enzymatic chain of methanogenesis<sup>6,7</sup>, while reducing equivalents are channelled to the partner SRB<sup>8,9</sup>.

However, natural gas generated by thermogenic decomposition of organic matter contains considerable amounts (up to 20%) short-chain alkanes including mostly ethane (up to 15%), but also propane, *iso*-butane and *n*-butane (hereafter butane)<sup>10,11</sup>. Although these gases are potential growth substrates for microorganisms, the anaerobic

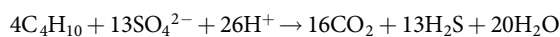
oxidation of the non-methane hydrocarbons became of interest only recently. All cultures known so far to oxidize short-chain hydrocarbons anaerobically are bacteria that couple complete substrate oxidation to CO<sub>2</sub> and sulfate reduction in one organism<sup>12–16</sup>. The only pure culture available so far is strain BuS5, a deltaproteobacterium<sup>12</sup>. Strain BuS5 and related organisms activate propane and butane via addition to fumarate yielding (1-methylalkyl)succinate, to date the most-studied anaerobic activation mechanism for hydrocarbons<sup>12,17–19</sup>. A recent study, however, suggests that this mechanism is not always involved in short-chain hydrocarbon oxidation<sup>20</sup>. Here we combined physiological experiments, community sequencing, microscopy, omics approaches and metabolite analyses to provide evidence for an alternative anaerobic activation reaction of butane in a highly enriched thermophilic culture of archaeal-bacterial consortia.

## Archaea catalyse thermophilic butane oxidation

Thermophilic anaerobic methanotrophic archaea (ANME-1) were previously found to be associated with a deltaproteobacterial phylotype, HotSeep-1<sup>9,21</sup> that had been detected independently in thermophilic enrichment cultures with short-chain alkanes<sup>12,15</sup>. This prompted us to attempt again thermophilic enrichments with a short-chain hydrocarbon, butane; for these, we used inocula from Guaymas Basin sediment samples that had already been incubated with methane and developed thermophilic AOM activity. Indeed, after two months, also butane-dependent sulfate reduction became obvious. Further cultivation and subsequent transfers to new medium with butane yielded a sediment-free culture, hereafter called Butane50. This culture reduced 10 mM sulfate within approximately 14 weeks of incubation. Quantitative growth experiments showed that the amount of butane degraded was apparently coupled to the stoichiometric reduction of

<sup>1</sup>Max-Planck Institute for Marine Microbiology, 28359 Bremen, Germany. <sup>2</sup>Alfred Wegener Institute Helmholtz Center for Polar and Marine Research, 27570 Bremerhaven, Germany. <sup>3</sup>MARUM, Center for Marine Environmental Sciences, University Bremen, 28359 Bremen, Germany. <sup>4</sup>Center for Biotechnology, Bielefeld University, 33615 Bielefeld, Germany. <sup>5</sup>Max Planck Institute for Biophysical Chemistry, 37077 Göttingen, Germany. <sup>6</sup>Helmholtz Centre for Environmental Research – UFZ, 04318 Leipzig, Germany. <sup>§</sup>current address: University of California at Santa Cruz, Ocean Sciences Department, Santa Cruz, CA 95064, USA.

sulfate to sulfide in a 1:3.25 ratio, as demonstrated also for strain BuS5 (Figure 1a; Supplementary Table 1), yielding the net reaction



In this culture the ANME-1 phylotype was no longer detectable by molecular analysis. Instead, archaea closely related to *Methanosarcinales* had become dominant due to the change to butane as substrate; they were members of the GoM-Arch87 clade<sup>22</sup> (Extended Data Table 1). Like ANME-1, also GoM-Arch87 forms densely packed consortia with the HotSeep-1 partner bacterium (Figure 1b,c). These consortia show strong blue-green autofluorescence (maximum at approx. 475 nm; Figure 1d), which is characteristic of cofactor F<sub>420</sub>, a hydrogen carrier typical for methanogenic and ANME archaea<sup>6,23</sup>. Phylotype GoM-Arch87 was originally detected in cold-seep areas of the Gulf of Mexico<sup>22</sup>, and since then was also found in other marine environments, especially seep and vent areas (see SILVA database release SSU 119; www.arb-silva.de). The environmental role of these archaea has been so far unknown.

From the metagenome assembly we retrieved two bins of contigs indicating genomes of two different GoM-Arch87 (Supplementary Table 2 and Extended Data Table 2). The two GoM-Arch87 bins have sizes of 1.46 Mbps (GoM-Arch87-1) and 1.66 Mbps (GoM-Arch87-2). Based on their tRNA content, archaeal specific single copy gene numbers and lineage-specific marker gene sets (*Euryarchaeota*) the draft genomes cover an estimated 85–89% of the complete genome of GoM-Arch87-1 and 95–97% of GoM-Arch87-2, indicating genome sizes of 1.64 to 1.71 Mbps. According to their 16S rRNA gene identity of 96% and whole genome identity of 74–90% (Figure 1e; Extended Data Table 2), the two bins likely represent different species of one genus. Hence we propose to name the more abundant (according to genome coverage) strain GoM-Arch87-1, *Candidatus* Syntrophoarchaeum butanivorans and the less abundant strain GoM-Arch87-2, *Candidatus* Syntrophoarchaeum caldarius. The two strains have largely similar gene content, and are further discussed together as *Ca.* Syntrophoarchaeum.

*Ca.* Syntrophoarchaeum encodes a fatty acid oxidation pathway, two complete acetyl-CoA decarboxylase/synthase:CO dehydrogenase (ACDS/CODH) complexes, and an almost complete methanogenesis-related pathway. Each of the two draft genomes contains four complete *mcr* gene sets, of which three (*Ca.* *S. butanivorans*) or all four (*Ca.* *S. caldarius*) are organized in operons (Extended Data Figure 1). The correct assembly and the unusually high number of *mcr* genes in a single genome were confirmed by cloning and resequencing each of the *mcrA* genes. Metatranscriptome and metaproteome analyses (only studied on *Ca.* *S. butanivorans*) showed that all these gene/protein sets were highly expressed/abundant (Extended Data Tables 3–5). Neither the metagenomic assembly nor the draft genomes of *Ca.* Syntrophoarchaeum contain genes encoding the otherwise wide-spread glycol radical enzymes (*assA/masD*, *bssA*) for anaerobic hydrocarbon activation. Accordingly, these genes could not be amplified from extracted DNA using specific primers (see methods). These results strongly indicated that the activation of butane in *Ca.* Syntrophoarchaeum proceeds via mechanisms different than those described for bacteria. An appealing hypothesis was that butane in *Ca.* Syntrophoarchaeum is activated by the distinct variants of MCR in a reaction analogous to that of methane at ‘reverse’ MCR in ANME. The expected first metabolite would thus be butyl-coenzyme M rather than methyl-coenzyme M.

### **Ca. Syntrophoarchaeum forms butyl-coenzyme M**

Analysis of cell extracts of active Butane50 cultures by direct infusion ultra-high resolution mass spectrometry indeed provided direct evidence for butane-dependent formation of butyl-coenzyme M. A mass peak of  $m/z = 197.03116$  was detected, which corresponded exactly to the hypothesized butyl-CoM ( $\text{C}_6\text{H}_{13}\text{S}_2\text{O}_3^-$ ). Following quadrupole isolation and collision-induced fragmentation this compound yielded two major fragments representing a butylthiol ( $m/z = 89.0430$ ,  $\text{C}_4\text{H}_9\text{S}^-$ ) and an apparently CoM-derived bisulfite ( $m/z = 80.9652$ ,  $\text{HSO}_3^-$ ; Figure 2

and Extended Data Figure 2a). Use of synthesized authentic standards showed that the two isomers, 1-butyl-CoM and 2-butyl-CoM, were present and separated by liquid chromatography, with apparently higher amounts of the latter (Figure 2c). The presence of two butyl-CoM isomers offers, in principle, two explanations. First, one could be the initial product whereas the other is the subsequently formed intermediate. Second, only one isomer may be the genuine, directly metabolized activation product, whereas the other is formed as a by-product due to relaxed catalytic specificity of the activating enzyme; this would be similar to the anaerobic activation of propane by strain BuS5, where both *n*- and *iso*-propylsuccinate have been detected as activation products<sup>12,24</sup>. Because the different amounts of the detected isomers reflect steady state concentrations (dynamic pools), they cannot offer clues to their metabolic significance. To further corroborate butyl-CoM formation as a specific activation reaction, i.e. exclude that it can be accomplished ‘accidentally’ by other means, we added butane to a methane-oxidizing ANME-1 enrichment. Neither butyl-CoM nor its derived fragments were detected. Moreover, these compounds were not detected in sterile controls, in substrate-starved Butane50 cultures, or in cultures of the bacterial butane-oxidizer strain BuS5 (Figure 2 and Extended Data Figure 2a).

Mechanistic relatedness between butane activation at the MCR variant and methane activation at MCR of methanotrophic archaea was also shown by an inhibition experiment. The coenzyme M analogue, bromoethanesulfonate (BES), which inhibits methanogenesis as well as anaerobic methane oxidation<sup>25</sup> also inhibited butane-dependent sulfate reduction (Extended Data Figure 3). Inhibition must occur in the archaeal metabolism, because BES did not affect the partner bacterium, HotSeep-1 (*Ca.* *Desulfofervidus auxilii*) when separately grown with hydrogen and sulfate; the tested partner originated from the thermophilic AOM culture<sup>26</sup>.

Aliquots of the Butane50 culture were also tested with other hydrocarbons. After approx. two months of incubation with propane, sulfate reduction became obvious. The rate increased and became similar as with butane. A possible shift in the microbial composition or gene expression upon incubation with propane has yet not been assessed. However, a mass peak exactly corresponding to that of propyl-CoM was analysed ( $m/z = 183.0155$ ; Extended Data Figure 2c). This further corroborates the formation of alkyl-CoM as the apparent initial product in short-chain alkane activation. So far, no sulfate reduction was detectable with added methane, ethane, *iso*-butane, *n*-pentane or *n*-hexane.

This is the first demonstration of coenzyme M acting *in vivo* as a carrier of alkyl moieties other than the methyl group. The closest known precedent is the *in vitro* reduction of the homologous substrate ethyl-CoM to ethane by MCR from methanogenic archaea<sup>27,28</sup>. Turnover rates of ethyl-CoM in these assays were two orders lower than of methyl-CoM, which was explained by a steric hindrance of the larger ethyl-CoM molecule in the MCR enzyme<sup>28</sup>. This suggests that an efficient activation of butane to butyl-CoM may require highly adapted MCR-like enzymes. Analysis of the deduced amino acid sequences of the eight *mcr* genes detected in *Ca.* Syntrophoarchaeum showed a low similarity among them with an identity of only 29–82%. Two different MCR enzymes encoded in the genome of *Ca.* *S. butanivorans* were highly abundant in protein extracts of the culture, qualifying them as likely candidates for butane activation (Extended Data Table 3).

A high substrate specificity of the MCR type apparently involved in butane oxidation was also indicated in an incubation experiment with both, butane and methane. In the active culture, butyl-CoM but no methyl-CoM was detected (Extended Data Figure 2b). Hence, there was no evidence for co-activation of methane, even though alone by its molecular size the latter should not encounter any steric binding hindrance. One may speculate that reaction at the enzyme requires substrate ‘fixation’ by binding of an alkyl chain of a minimum length. Understanding as to which extent the slightly weaker C—H-bond in higher alkanes in comparison to that in methane could play a role may need refined theoretical consideration. Furthermore, the population

and abundant MCR type in the recent propane-adapted subculture will have to be analysed. At the present state it is unknown whether propane and butane are activated by the same organism and enzyme or cause selection of different ones with respective substrate preference.

Notably three of the McrA subunits of *Ca. S. butanivorans* have a related equivalent in *Ca. S. caldarius*. Interestingly the fourth McrA subunit (SBU\_000314) forms a cluster with McrA sequences of the recently described *Bathyarchaeota*<sup>29</sup>, whereas the fourth sequence of *Ca. S. caldarius* (SCAL\_000352) has a distant phylogenetic position (Figure 3; for further phylogenetic analysis see Methods and Supplementary Figure 1). Together McrA sequences of *Ca. Syntrophoarchaeum* and *Bathyarchaeota* form a highly divergent cluster compared to those of methanogens or methanotrophs, which is likely due to the ability of the encoded enzymes to efficiently accommodate larger substrates such as butane.

### Complete oxidation of butane

The measured stoichiometric balance shows that the CoM-bound butyl moiety must be completely degraded to CO<sub>2</sub>. Only a minor fraction is expected to enter biosynthesis, like in other strict anaerobes<sup>30</sup>. Complete oxidation requires four basic metabolic features, the conversion of the butyl-thioether to the butyryl-thioester (presumably butyryl-CoA), oxidation of butyryl-CoA to acetyl-CoA, terminal oxidation of acetyl-CoA to CO<sub>2</sub>, and channelling of the reducing equivalents (electrons) into sulfate reduction. Our proteogenomic analysis provides explanations for all of these processes, with the exception of the first.

The role and significance of the butyl-CoM isomers and their subsequent processing steps could not be clarified on the basis of our present analyses. Also, there are no precedent cases of natural pathways involving non-methyl CoM-thioethers that could suggest particular reactions. Still, one may argue that 1-butyl-CoM is the genuine and directly metabolized activation product. Because MCR in AOM activates a primary C—H-bond, its variant in culture Butane50 may also attack butane at the primary carbon. In this way, first oxidation and functionalization would occur at the same carbon atom which in a subsequent beta-oxidation would become the activated carboxyl group (thioester). In such case, 2-butyl-CoM would be a by-product; it is presently unknown whether an isomerase converts it to 1-butyl-CoM.

In methyl-CoM oxidation in AOM and in the oxidative branch in methanol-grown *Methanosarcina*, the subsequent steps would be transfer of the methyl group to tetrahydromethanopterin (H<sub>4</sub>MPT) or tetrahydroscarinapterin (H<sub>4</sub>SPT) and oxidation via the bound formaldehyde and formate states finally to CO<sub>2</sub>. None of the genes encoding methyl-H<sub>4</sub>MPT:coenzyme M methyltransferase were found in the genome. An analogous transfer of the butyl-moiety by the abundant, presumably modified methyltransferase (Mta) may be only speculated about (Figure 4, Extended Data Table 3), because the postulated butyl-cobalamin intermediate would be unprecedented. Furthermore, tetrahydropterins and methanofuran are, to our knowledge, exclusive C<sub>1</sub>-carriers. Hence, the enzymatic reactions converting 1-butyl-CoM to the butyryl (bound acid) level are presently puzzling, even though transfer and oxidation reactions of higher carbon compounds can be theoretically formulated also with the C<sub>1</sub>-carriers.

The predicted beta oxidation enzymes of *Ca. Syntrophoarchaeum* (Figure 4, Extended Data Table 3) are highly related to those of delta-proteobacterial sulfate reducers and syntrophic partners of methanogens<sup>31,32</sup> (Extended Data Table 6). This suggests horizontal gene transfer across the two domains of life. The gene encoding the most abundantly formed acyl-CoA dehydrogenase of *Ca. Syntrophoarchaeum* is located in an operon with genes for an electron transfer flavoprotein (*etf*) complex and a [FeS]-oxidoreductase. Hence, these gene products likely act as electron acceptors in the oxidation of butyryl-CoA (Figure 4) as previously shown for bacterial butyrate oxidizers<sup>33,34</sup>.

The key enzyme for the metabolism of acetyl-CoA from beta-oxidation is the detected acetyl-CoA decarboxylase/synthase:CO

dehydrogenase (ACDS/CODH). The carboxyl group-derived bound CO can be oxidized to free CO<sub>2</sub> and yield reduced ferredoxin as shown before for methanogens<sup>23</sup>. The methyl group is probably oxidized via the reverse methanogenesis pathway, of which almost all genes are present and their corresponding transcripts and proteins were detected (Figure 4, Extended Data Table 4). The N<sub>5</sub>,N<sub>10</sub>-methylene-tetrahydromethanopterin (methylene-H<sub>4</sub>MPT) reductase (*mer*) gene is absent in *Ca. Syntrophoarchaeum*. However, like in ANME-1 Mer could be substituted by the highly abundant putative methylenetetrahydrofolate reductase (Met) complex as suggested before<sup>35</sup>. The genes encoding the Met complex of *Ca. Syntrophoarchaeum* have a similar operon structure to those of *Moorella thermoacetica*<sup>36</sup>. In conclusion, the combination of enzymes in *Ca. Syntrophoarchaeum* results in the archaeal version of the oxidative Wood-Ljungdahl pathway, as originally shown for the sulfate-reducing *Archaeoglobus fulgidus*<sup>37</sup>.

*Ca. Syntrophoarchaeum* does not have the genes for canonical sulfate reduction (i.e. *dsrAB*, *aprAB*), and hence depends on an external electron sink. This role is apparently fulfilled by the partner bacterium. We tested for the production of hydrogen as a canonical intermediate in syntrophic associations. Although *Ca. Syntrophoarchaeum* encodes for a cytoplasmic [NiFe] hydrogenase (Extended Data Table 5), only minor amounts of hydrogen were produced in active or molybdate-treated Butane50 cultures, which cannot explain the required reducing equivalent transfer (Figure 5a). To further study how reducing equivalents are transferred to the partner bacterium, the draft genome of the Butane50 HotSeep-1 strain was retrieved from the metagenome. Based on different marker genes, this HotSeep-1 strain is basically identical to *Ca. D. auxilii*, the partner in thermophilic AOM<sup>26</sup> (Supplementary Table 3). *Ca. D. auxilii* is a lithoautotrophic sulfate reducer that in thermophilic AOM thrives on electrons directly supplied by the ANME via pili-based nanowires and cytochromes<sup>9,26</sup>. Also in the Butane50 culture HotSeep-1 expresses genes encoding pili assembly proteins, especially the main component of type IV pilus (PilA), and many different potentially cytochromes including extracellular ones (Extended Data Table 7). Indeed, using transmission electron microscopy we found a similarly dense, apparently pili-based, nanowire network in the intercellular space of the Butane50 consortia (Figure 5b). Based on these results we propose that nanowire-based direct interspecies electron transfer<sup>38</sup> mediates also electron exchange in the butane-oxidizing consortia. From a thermodynamic point of view, the interspecies transfer of reducing equivalents would be also possible via H<sub>2</sub>; its measured partial pressure of ca. 1 Pa would allow energy conservation in both partners, albeit with quite unequal energy sharing (calculation in Supplementary Discussion; Supplementary Figure 2). However, the extremely slow rate of H<sub>2</sub> formation (Figure 5a) is difficult to reconcile with the observed rate of sulfate reduction.

Channelling of the reducing equivalents to the sulfate-reducing partner bacterium requires electrons with redox potentials below the average potential of sulfate reduction ( $E^{\circ} = -220$  mV), which is reached by most proposed redox reactions. However, the oxidation of butyryl-CoA to crotonyl-CoA (Figure 4), will release electrons with far higher potentials ( $E^{\circ} = -125/-10$  mV<sup>33</sup>). A shift in the redox potential of these electrons can be achieved by different mechanisms, including energy-driven reverse electron transport<sup>33</sup> or electron confurcation<sup>39</sup>, both demonstrated for syntrophic bacteria. Two of the required genes, encoding EtFAB and FeS oxidoreductase, were identified in *Ca. Syntrophoarchaeum*. Other genes with products involved in electron transport have been identified including different heterodisulfide reductases (Extended Data Table 5) like one complex of HdrABC (SBUT\_000297-299) followed by the genes encoding the  $\beta$ -subunit of formate dehydrogenase (FdhB) and the  $\delta$ -subunit of methylviologen-reducing hydrogenase (MvhD) (Extended Data Table 5). This complex was already identified in ANME-1 genomes and was hypothesised to be involved as electron-accepting complex<sup>7</sup>.

## Evolutionary and environmental aspects

The analysis of the anaerobic consortia enriched with butane provides first insights into an additional mechanism for the oxygen-independent activation and use of non-methane saturated hydrocarbons in archaea. Saturated hydrocarbons belong to the chemically least reactive compounds. In anaerobic bacteria, the radical-catalysed addition of alkanes to fumarate yielding substituted succinates is regarded as common<sup>40,41</sup>, even though alternative mechanisms have been proposed<sup>42,43</sup>. The MCR-like proteins produced by *Ca. Syntrophoarchaeum* and formation of butyl-coenzyme M in the culture suggest that the mechanistic principle for the activation of methane, the most stable hydrocarbon, was evolutionarily adapted to use also short chain alkanes. Another requirement for metabolic processing was, apart from the yet unsolved subsequent step of the alkyl-thioether, the acquisition of enzymes for beta-oxidation, which has been shown before in other archaea<sup>44</sup>. The subsequent reactions leading to CO<sub>2</sub> are enabled by steps which in principle are long-known in methanogens; acetate- and methanol-utilizing species contain CO-dehydrogenase/acetyl-CoA synthase as well as C<sub>1</sub>-processing enzymes able to operate in oxidative direction<sup>45</sup>. Such an archaeal variant of the Wood-Ljungdahl pathway for acetyl-CoA oxidation was first described for the sulfate reducer *Archaeoglobus fulgidus*<sup>37</sup>.

The presently suggested pathway for anaerobic oxidation of non-methane alkanes might not be limited to *Ca. Syntrophoarchaeum*. The recently detected uncultivated *Bathyarchaeota* contain genes for MCR types highly similar to those of *Ca. Syntrophoarchaeum* (Figure 3). Furthermore, the draft genomes of *Bathyarchaeota*<sup>29</sup> as well as the pan-genome of uncultivated *Hadesarchaea*<sup>46</sup> encode most enzymes of the methanogenesis pathway, for short-chain fatty acid oxidation and for acetyl-CoA oxidation via ACDS/CODH. Based on these predicted features, *Bathyarchaeota* were described as heterotrophic methanogens. Our results indicate that at least some of these uncultivated archaea may be also viewed as alkane oxidizers.

In conclusion, anaerobic microorganisms thriving on non-methane alkanes may be phylogenetically and metabolically even more diverse than hitherto thought<sup>47,48</sup>. Such diversity may reflect a long-existing presence of saturated hydrocarbons in the biosphere and their exploitation as growth substrates through various evolving pathways, long before the oxygen-dependent ones. The factors which in modern anoxic environments select for consortial, archaeal hydrocarbon oxidation over an oxidation by single bacterial species<sup>12,41</sup> are still unknown and need more comprehensive *in situ* studies.

**Online Content** Methods, along with any additional Extended Data display items and Source Data, are available in the online version of the paper; references unique to these sections appear only in the online paper.

Received 6 June; accepted 11 October 2016.

Published online 17 October 2016.

1. Simoneit, B. R. T., Kawka, O. E. & Brault, M. Origin of Gases and Condensates in the Guaymas Basin Hydrothermal System (Gulf of California). *Chemical geology* **71**, 169–182, doi:10.1016/0009-2541(88)90113-1 (1988).
2. Reeburgh, W. Oceanic methane biogeochemistry. *Chem Rev.* **107**, 486–513 (2007).
3. Boetius, A. & Wenzhofer, F. Seafloor oxygen consumption fuelled by methane from cold seeps. *Nature Geoscience* **6**, 725–734, doi:10.1038/NGEO1926 (2013).
4. Orphan, V. J., House, C. H., Hinrichs, K. U., McKeegan, K. D. & DeLong, E. F. Methane-consuming archaea revealed by directly coupled isotopic and phylogenetic analysis. *Science* **293**, 484–487, doi:10.1126/science.1061338 (2001).
5. Boetius, A. *et al.* A marine microbial consortium apparently mediating anaerobic oxidation of methane. *Nature* **407**, 623–626, doi:10.1038/35036572 (2000).
6. Hallam, S. J. *et al.* Reverse methanogenesis: testing the hypothesis with environmental genomics. *Science* **305**, 1457–1462, doi:10.1126/science.1100025 (2004).
7. Meyerdierks, A. *et al.* Metagenome and mRNA expression analyses of anaerobic methanotrophic archaea of the ANME-1 group. *Environ Microbiol* **12**, 422–439, doi:10.1111/j.1462-2920.2009.02083.x (2010).
8. McGlynn, S. E., Chadwick, G. L., Kempes, C. P. & Orphan, V. J. Single cell activity reveals direct electron transfer in methanotrophic consortia. *Nature advance online publication*, doi:10.1038/nature15512 (2015).

9. Wegener, G., Krukenberg, V., Riedel, D., Tegetmeyer, H. E. & Boetius, A. Intercellular wiring enables electron transfer between methanotrophic archaea and bacteria. *Nature* **526**, 587–590 (2015).
10. Claypool, G. E. & Kvenvolden, K. A. Methane and Other Hydrocarbon Gases in Marine Sediment. *Annu Rev Earth Planet Sc* **11**, 299–327, doi:DOI 10.1146/annurev.ea.11.050183.001503 (1983).
11. Tissot, B. P. & Welte, D. H. *Petroleum formation and occurrence*. (Springer-Verlag, 1984).
12. Kniermeyer, O. *et al.* Anaerobic oxidation of short-chain hydrocarbons by marine sulphate-reducing bacteria. *Nature* **449**, 898–901, doi:10.1038/nature06200 (2007).
13. Savage, K. N. *et al.* Biodegradation of low-molecular-weight alkanes under mesophilic, sulfate-reducing conditions: metabolic intermediates and community patterns. *FEMS Microbiol Ecol* **72**, 485–495 (2010).
14. Jaekel, U. *et al.* Anaerobic degradation of propane and butane by sulfate-reducing bacteria enriched from marine hydrocarbon cold seeps. *ISME J* **7**, 885–895, doi:10.1038/ismej.2012.159 (2013).
15. Adams, M. M., Hoarfrost, A. L., Bose, A., Joye, S. B. & Girguis, P. R. Anaerobic oxidation of short-chain alkanes in hydrothermal sediments: potential influences on sulfur cycling and microbial diversity. *Front. Microbiol.* **4**, 110, doi:10.3389/fmicb.2013.00110 (2013).
16. Kleindienst, S. *et al.* Diverse sulfate-reducing bacteria of the Desulfosarcina/Desulfococcus clade are the key alkane degraders at marine seeps. *ISME J* **8**, 2029–2044, doi:10.1038/ismej.2014.51 (2014).
17. Kropp, K. G., Davidova, I. A. & Suflija, J. M. Anaerobic oxidation of n-dodecane by an addition reaction in a sulfate-reducing bacterial enrichment culture. *Applied and environmental microbiology* **66**, 5393–5398 (2000).
18. Rabus, R. *et al.* Anaerobic initial reaction of n-alkanes in a denitrifying bacterium: evidence for (1-methylpentyl) succinate as initial product and for involvement of an organic radical in n-hexane metabolism. *Journal of Bacteriology* **183**, 1707–1715 (2001).
19. Heider, J. *et al.* Structure and function of benzylsuccinate synthase and related fumarate-adding glycol radical enzymes. *Journal of Molecular Microbiology and Biotechnology* **26**, 29–44 (2016).
20. Gittel, A. *et al.* Ubiquitous presence and novel diversity of anaerobic alkane degraders in cold marine sediments. *Frontiers in Microbiology* **6** (2015).
21. Holler, T. *et al.* Thermophilic anaerobic oxidation of methane by marine microbial consortia. *ISME J* **5**, 1946–1956, doi:10.1038/ismej.2011.77 (2011).
22. Orcutt, B. N. *et al.* Impact of natural oil and higher hydrocarbons on microbial diversity, distribution, and activity in Gulf of Mexico cold-seep sediments. *Deep-Sea Research Part II-Topical Studies in Oceanography* **57**, 2008–2021, doi:10.1016/j.dsr2.2010.05.014 (2010).
23. Thauer, R. Biochemistry of methanogenesis: a tribute to Marjory Stephenson. 1998 Marjory Stephenson Prize Lecture. *Microbiology* **144**, 2377–2406 (1998).
24. Jaekel, U., Vogt, C., Fischer, A., Richnow, H.-H. & Musat, F. Carbon and hydrogen stable isotope fractionation associated with the anaerobic degradation of propane and butane by marine sulfate-reducing bacteria. *Environmental Microbiology* **16**, 130–140, doi:10.1111/1462-2920.12251 (2014).
25. Nauhaus, K., Treude, T., Boetius, A. & Kruger, M. Environmental regulation of the anaerobic oxidation of methane: a comparison of ANME-I and ANME-II communities. *Environ Microbiol* **7**, 98–106 (2005).
26. Krukenberg, V. *et al.* Candidatus Desulfofervidus auxilii, a hydrogenotrophic sulfate-reducing bacterium of the HotSeep-1 cluster involved in the thermophilic anaerobic oxidation of methane. *Environ Microbiol* (2016).
27. Ahn, Y., Krzycki, J. A. & Floss, H. G. Steric course of the reduction of ethyl coenzyme M to ethane catalyzed by methyl coenzyme M reductase from *Methanosarcina barkeri*. *Journal of the American Chemical Society* **113**, 4700–4701 (1991).
28. Scheller, S., Goenrich, M., Thauer, R. K. & Jaun, B. Methyl-coenzyme M reductase from methanogenic archaea: isotope effects on label exchange and ethane formation with the homologous substrate ethyl-coenzyme M. *J. Am. Chem. Soc* **135**, 14985–14995 (2013).
29. Evans, P. N. *et al.* Methane metabolism in the archaeal phylum Bathyarchaeota revealed by genome-centric metagenomics. *Science* **350**, 434–438, doi:10.1126/science.aac7745 (2015).
30. Nauhaus, K., Albrecht, M., Elvert, M., Boetius, A. & Widdel, F. In vitro cell growth of marine archaeal-bacterial consortia during anaerobic oxidation of methane with sulfate. *Environ Microbiol* **9**, 187–196 (2007).
31. McInerney, M., Bryant, M., Hespell, R. & Costerton, J. *Syntrophomonas wolfei* gen. nov. sp. nov., an anaerobic, syntrophic, fatty acid-oxidizing bacterium. *Applied and environmental microbiology* **41**, 1029–1039 (1981).
32. Schmidt, J. E. & Ahring, B. K. Effects of hydrogen and formate on the degradation of propionate and butyrate in thermophilic granules from an upflow anaerobic sludge blanket reactor. *Applied and environmental microbiology* **59**, 2546–2551 (1993).
33. Schmidt, A., Müller, N., Schink, B. & Schleheck, D. A proteomic view at the biochemistry of syntrophic butyrate oxidation in *Syntrophomonas wolfei*. *PLoS one* **8**, e56905 (2013).
34. Wasmund, K. *et al.* Genome sequencing of a single cell of the widely distributed marine subsurface Dehalococcoidia, phylum Chloroflexi. *ISME J* **8**, 383–397, doi:10.1038/ismej.2013.143 (2014).
35. Stokke, R., Roalkvam, I., Lanzen, A., Hafliadason, H. & Steen, I. H. Integrated metagenomic and metaproteomic analyses of an ANME-1-dominated community in marine cold seep sediments. *Environ Microbiol* **14**, 1333–1346, doi:10.1111/j.1462-2920.2012.02716.x (2012).

36. Mock, J., Wang, S., Huang, H., Kahnt, J. & Thauer, R. K. Evidence for a hexaheteromeric methylenetetrahydrofolate reductase in *Moorella thermoacetica*. *Journal of Bacteriology* **196**, 3303–3314 (2014).
37. Möller-Zinkhan, D. & Thauer, R. K. Anaerobic lactate oxidation to 3 CO<sub>2</sub> by *Archaeoglobus fulgidus* via the carbon monoxide dehydrogenase pathway: demonstration of the acetyl-CoA carbon-carbon cleavage reaction in cell extracts. *Archives of microbiology* **153**, 215–218 (1990).
38. Summers, Z. M. *et al.* Direct Exchange of Electrons Within Aggregates of an Evolved Syntrophic Coculture of Anaerobic Bacteria. *Science* **330**, 1413–1415, doi:10.1126/science.1196526 (2010).
39. Weghoff, M. C., Bertsch, J. & Müller, V. A novel mode of lactate metabolism in strictly anaerobic bacteria. *Environmental Microbiology* **17**, 670–677 (2015).
40. Callaghan, A. V. Metabolomic investigations of anaerobic hydrocarbon-impacted environments. *Curr Opin Biotech* **24**, 506–515, doi:10.1016/j.copbio.2012.08.012 (2013).
41. Musat, F. The anaerobic degradation of gaseous, nonmethane alkanes—From in situ processes to microorganisms. *Computational and structural biotechnology journal* **13**, 222–228 (2015).
42. So, C. M., Phelps, C. D. & Young, L. Anaerobic transformation of alkanes to fatty acids by a sulfate-reducing bacterium, strain Hxd3. *Appl. Environ. Microbiol.* **69**, 3892–3900 (2003).
43. Heider, J., Szalaniec, M., Suenwoldt, K. & Boll, M. Ethylbenzene dehydrogenase and related molybdenum enzymes involved in oxygen-independent alkyl chain hydroxylation. *Journal of Molecular Microbiology and Biotechnology* **26**, 45–62 (2016).
44. Klenk, H.-P. *et al.* The complete genome sequence of the hyperthermophilic, sulphate-reducing archaeon *Archaeoglobus fulgidus*. *Nature* **390**, 364–370 (1997).
45. Ferry, J. G. Biochemistry of methanogenesis. *Critical Reviews in Biochemistry and Molecular Biology* **27**, 473–503 (1992).
46. Baker, B. J. *et al.* Genomic inference of the metabolism of cosmopolitan subsurface Archaea, Hadesarchaea. *Nature Microbiology*, 16002, doi:10.1038/nmicrobiol.2016.2(2016).
47. Stagars, M. H., Ruff, S. E., Amann, R. & Knittel, K. High diversity of anaerobic alkane-degrading microbial communities in marine seep sediments based on (1-methylalkyl) succinate synthase genes. *Frontiers in Microbiology* **6** (2015).
48. Rabus, R., Boll, M., Golding, B. & Wilkes, H. Anaerobic Degradation of p-Alkylated Benzoates and Toluenes. *Journal of Molecular Microbiology and Biotechnology* **26**, 63–75 (2016).

**Supplementary Information** is available in the online version of the paper.

**Acknowledgements** We thank Ramona Appel, Kathrin Büttner, Ines Kattelmann and Susanne Menger for assistance in cultivation and molecular work, Benjamin Scheer for proteomic analyses, and Marcel Sickert, Jakob Then Bergh and Kristina Dürkop for support in standard synthesis and LC-MS/MS analyses. We thank as well Antonio Fernández-Guerra, Harald Gruber-Vodicka and Pierre Offre for supporting us in bioinformatics and biochemistry. We thank Antje Boetius for fruitful discussions and financial support by her Leibniz Grant of the Deutsche Forschungsgemeinschaft (DFG). Research was further financed by the DFG Research Center and Cluster of Excellence MARUM and the Deep Carbon Observatory (Deep Life grant 11121/6152-2121-2329-9973-CC to G.W.), the Max Planck Society and the Helmholtz Society. We are indebted to Andreas Teske and the shipboard party, the crew and pilots of research expedition AT15-16 Research Vessel Atlantis and Research Submersible Alvin (NSF Grant OCE-0647633). We acknowledge the Centre for Chemical Microscopy (ProVIS) at the Helmholtz Centre for Environmental Research supported by European regional Development Funds (EFRE – Europe funds Saxony) for using their analytical facilities.

**Author Contributions** G.W. and F.M. retrieved the original samples and performed cultivation. R.L.-P., G.W., and F.M. designed research. R.L.-P., K.K., K.J.H. and V.K. designed the CARD-FISH probes and performed microscopy. R.L.-P., G.W. and F.M. performed physiological experiments. H.E.T. prepared and sequenced the DNA and RNA libraries. R.L.-P., V.K., D.V.M. and M.R. performed metagenomic and transcriptomic analyses. R.L.-P., K.K. and K.J.H. performed phylogenetic analysis. D.R. performed thin-sectioning and electron microscopy. H.-H.R., L.A. and F.M. performed proteome analyses. T.R., O.L. and F.M. analysed metabolic intermediates. R.L.-P., G.W., F.W. and F.M. developed the metabolic model, and wrote the manuscript with contributions of all co-authors.

**Author Information** Reprints and permissions information is available at [www.nature.com/reprints](http://www.nature.com/reprints). The authors declare competing financial interests. Readers are welcome to comment on the online version of the paper. Correspondence and requests for materials should be addressed to G.W. ([gwegener@mpi-bremen.de](mailto:gwegener@mpi-bremen.de)) or F.M. ([florin.musat@ufz.de](mailto:florin.musat@ufz.de))

**Reviewer Information** *Nature* thanks T. Ettema, S. Ragsdale, R. Thauer and the other anonymous reviewer(s) for their contribution to the peer review of this work..

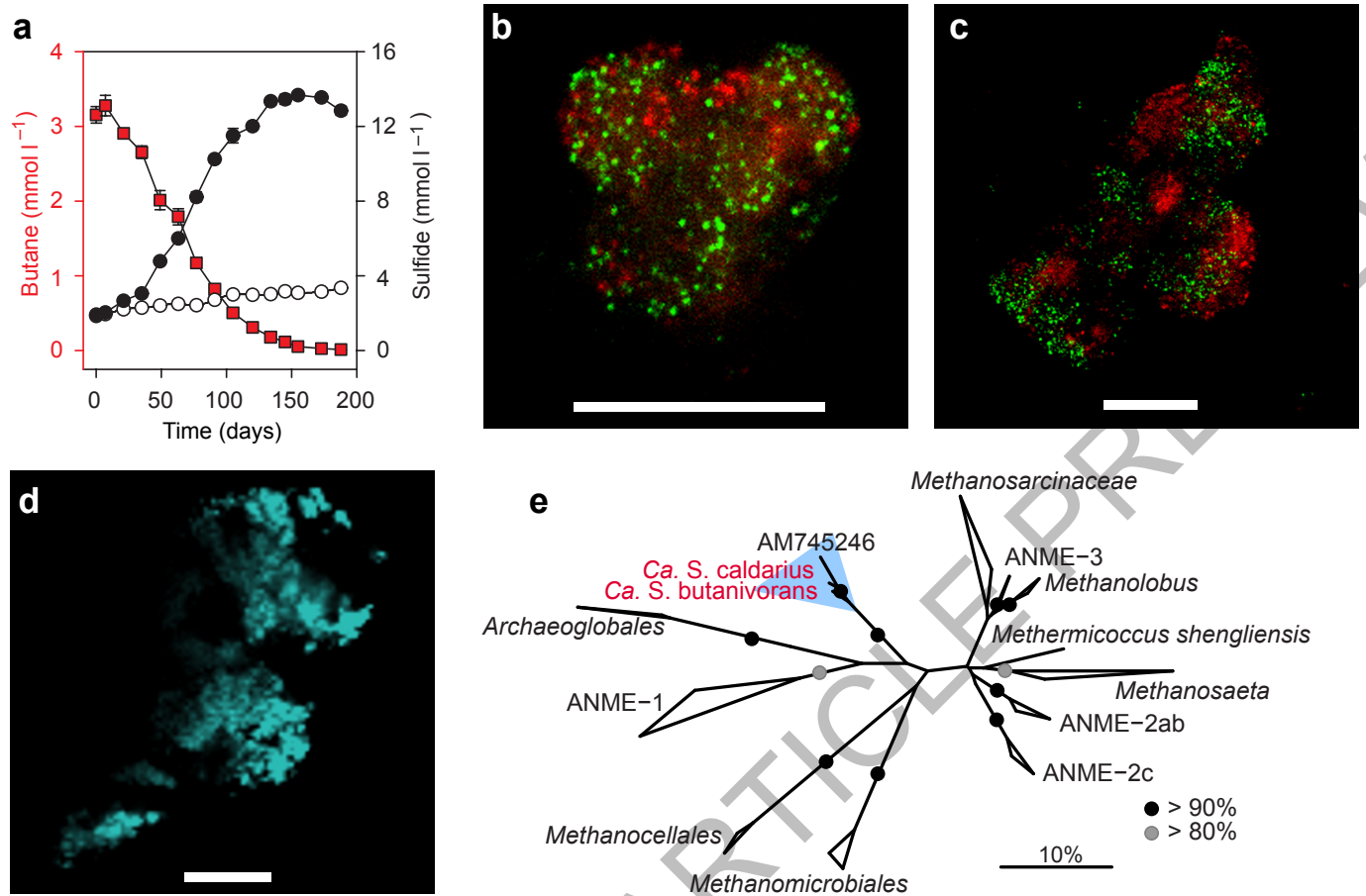


**Figure 1 | Characterization of the Butane50 culture.** **a**, The Butane50 culture consumed butane (red squares) coupled with stoichiometric reduction of sulfate to sulfide (black circles); no sulfide was produced in cultures without butane (white circles), error bar = standard deviation,  $n = 3$ . **b,c**, Fluorescence micrographs of Butane50 consortia stained with specific probes for GoM-Arch87 (red) and HotSeep-1 (green); representative for 20 recorded images, scale bar = 10  $\mu\text{m}$ . **d**, Autofluorescence of microbial consortia visualized using excitation

light at 405 nm and a longpass emission filter (>463 nm). The autofluorescence maximum at 470 nm is indicative of the presence of the cofactor  $F_{420}$ ; representative for 10 recorded images, scale bar = 10  $\mu\text{m}$ . **e**, Phylogenetic affiliation of the 16S rRNA gene sequences from the studied *Ca. Syntrophoarchaeum* strains (in red) within the *Euryarchaeota*. The GoM-Arch87 cluster is indicated with blue background; bar = 10% estimated sequence divergence; bootstraps values >80% and >90% are indicated by grey and black circles, respectively.

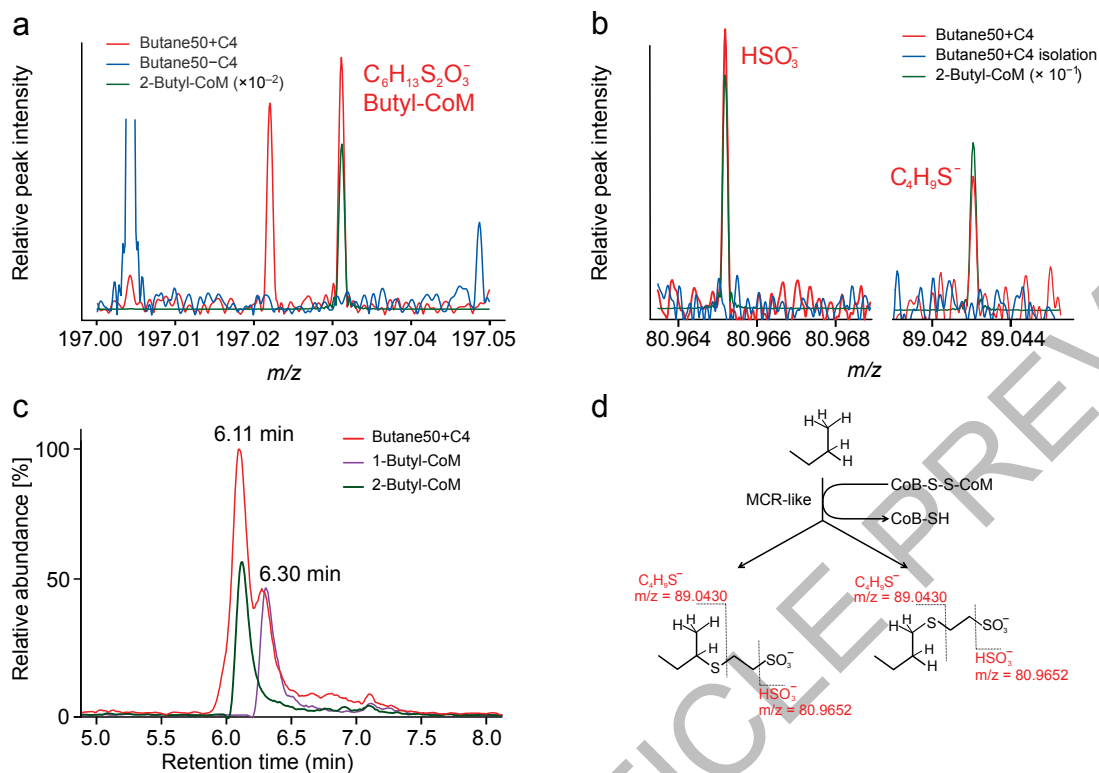


**Figure 2 | Butyl-CoM as initial metabolic intermediate in butane oxidation** **a**, Full scan mass spectrum of Butane50 culture extracts (Butane50+C4;  $n = 6$  at different time points) revealed a peak at  $m/z = 197.0312$  which matches the butyl-CoM standard (mass accuracy  $+0.18$  ppm). This mass peak was absent in control incubations without butane (Butane50-C4; for more controls see Extended Data Figure 2). **b**, Isolation and collision induced fragmentation of this mass peak yielded

butylthiol (mass accuracy  $+0.01$  ppm) and bisulfite (mass accuracy  $+0.03$  ppm), which are likewise produced by fragmentation of the butyl-CoM standards. **c**, Liquid chromatography resolved the presence of the two isomers 1- and 2-butyl-CoM in the culture ( $n = 4$  at different sulfide concentrations). **d**, Interpretation of these analyses. Butane is activated by ligation to coenzyme M by MCR-like enzymes, yielding both 1- and 2-butyl-CoM with identical fragmentation patterns.

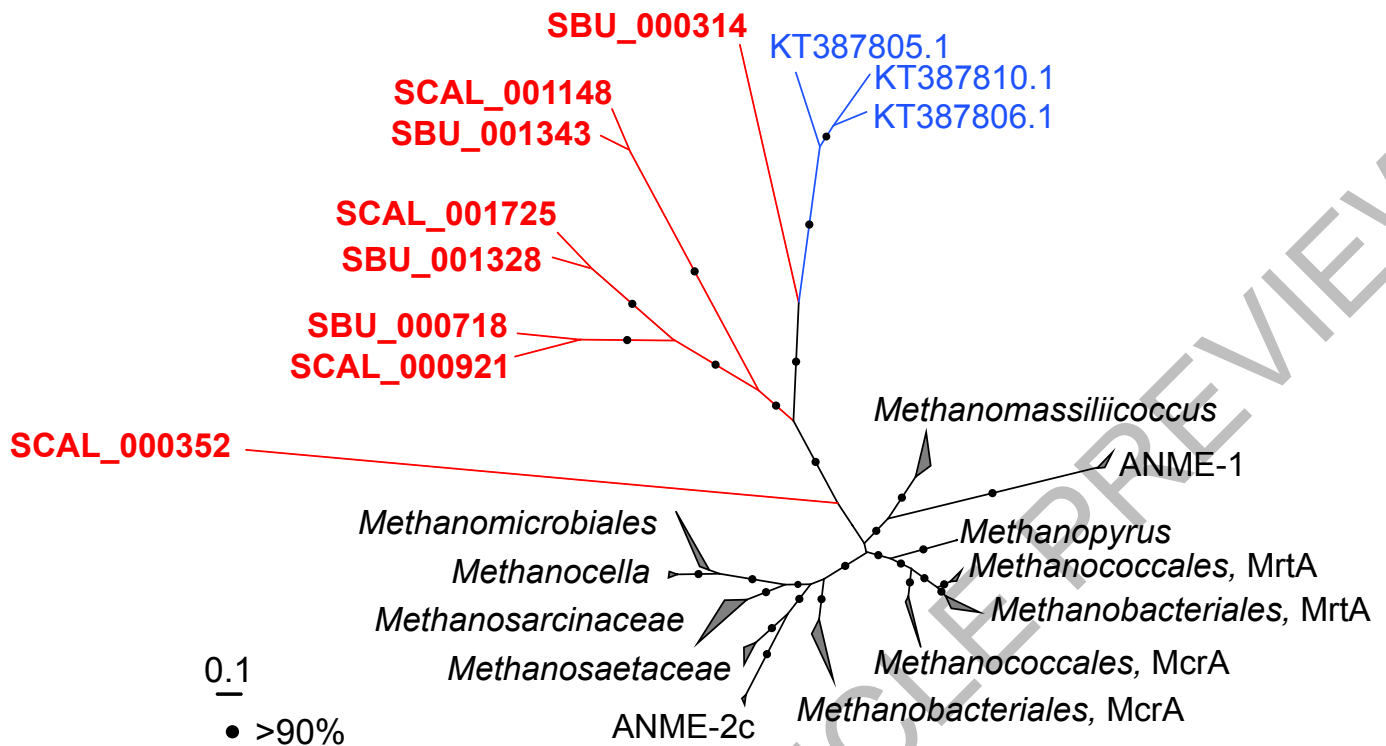


**Figure 3 | Phylogenetic affiliation of McrA amino acid sequences present in *Ca. S. butanivorans* and *Ca. S. caldarius*.** The phylogenetic tree was constructed based on a maximum likelihood algorithm considering more than 500 amino acid positions. Red branches = sequences from *Ca. Syntrophoarchaeum*; SBU = *Ca. S. butanivorans*; SCAL = *Ca. S. caldarius*, the identifiers refer to the

locus tag of the sequences in the draft genomes. Blue branches indicate *Bathyarchaeota* related sequences from Evans et al<sup>29</sup>. The scale bar indicates the number of amino acid substitutions per site. Bootstrap values higher than 90% are indicated by filled circles on the corresponding branch.

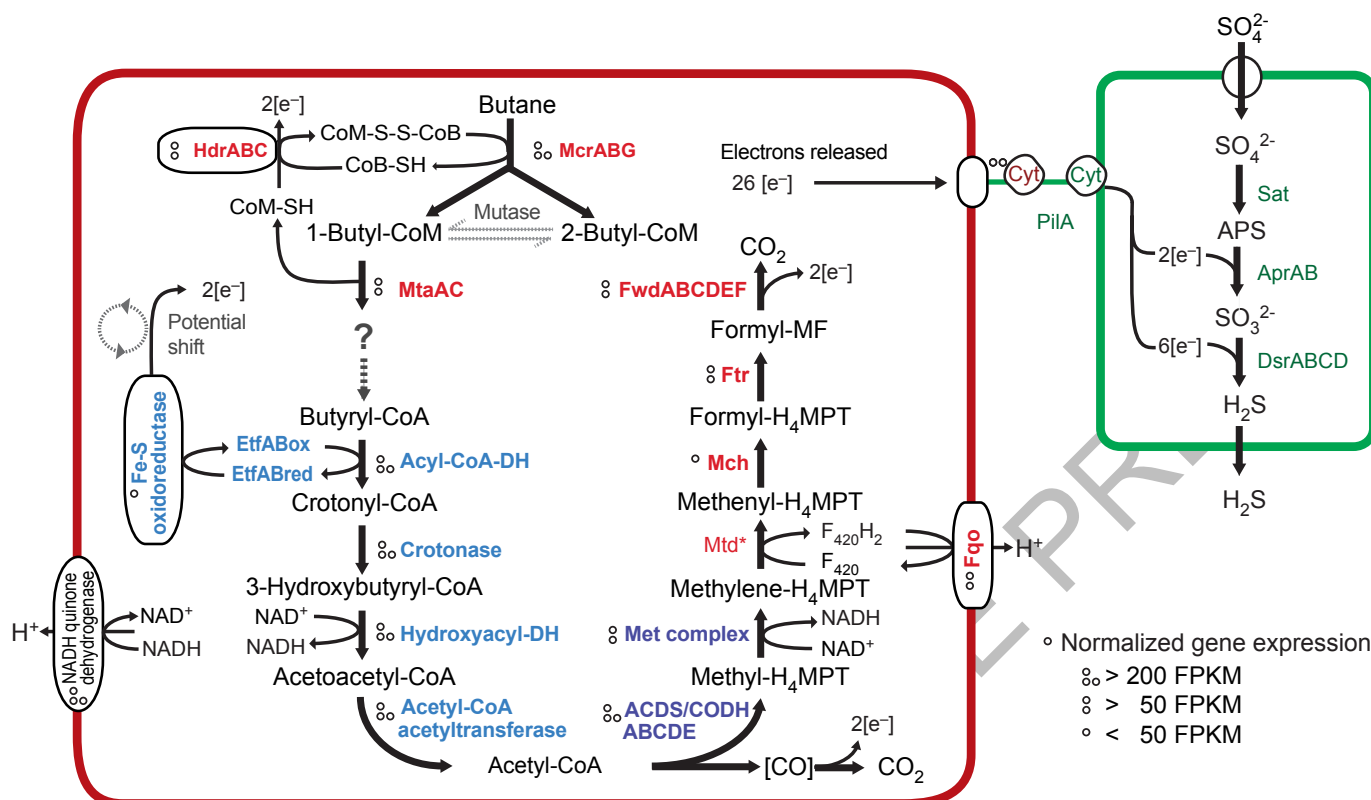


**Figure 4 | Metabolic scheme proposed for butane oxidation with sulfate based on molecular analyses.** *Ca. Syntrophoarchaeum* (red cell) uses steps of the methanogenesis pathway (red labels) to activate butane and to oxidize methylene-tetrahydromethanopterin to CO<sub>2</sub>. Butyryl-CoA oxidation is catalysed by enzymes shared with syntrophic bacteria (blue labels). Acetyl-CoA is oxidized by a reverse Wood-Wjungdahl pathway (violet labels). Reducing equivalents are transferred via cytochromes (produced by both organisms) and pili-based nanowires to the sulfate-reducing HotSeep-1 partner bacterium (green cell and labels). Normalized

gene expression for *Ca. S. butanivorans* is indicated as FPKM (Fragments Per Kilobase of transcript per Million mapped reads) according to the legend code; enzyme names in boldface indicate their detection in protein extracts; dotted arrows mark hypothetical pathways without detected genes; \**mtd* has only been detected in the more complete genome of *Ca. S. caldarius*. Symbol [e<sup>-</sup>] indicates electrons bound to heme or [FeS]-clusters in proteins, or to unknown or non-specified carriers. H<sub>2</sub>O, energy conservation and biosynthesis are not indicated.

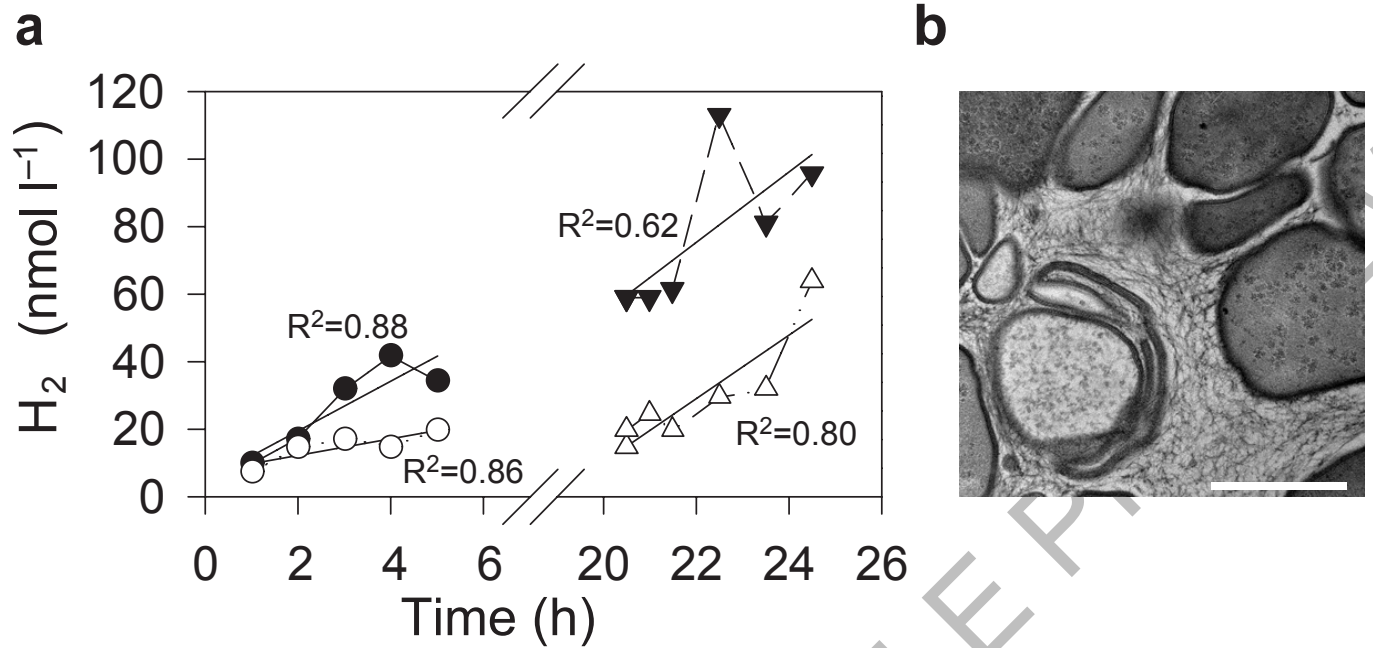


**Figure 5 | Testing metabolic interaction of *Ca. Syntrophoarchaeum* and *Ca. D. auxilii* in Butane50 cultures. a**, Development of hydrogen concentration in replicate active Butane50 cultures ( $n = 2$ ) without (circles) and next day continuation with molybdate addition (10 mM final concentration; triangles) to inhibit sulfate reduction. H<sub>2</sub> production was between 3–7 nmol l<sup>-1</sup> h<sup>-1</sup> and therefore 3–4 orders of magnitude

below a potential hydrogen production of 46,000 nmol l<sup>-1</sup> h<sup>-1</sup> if H<sub>2</sub> was the intermediate (determined from the measured sulfate reduction rate of 276  $\mu\text{mol l}^{-1} \text{d}^{-1}$  before the experiments). **b**, Transmission electron micrograph of an EPON 812 embedded consortium thin-section. The intercellular space in the consortium is filled with abundant nanowire-like structures; scale bar = 0.5  $\mu\text{m}$ , representative for >30 recorded images.

## METHODS

**Origin of inoculum and cultivation of the Butane50 enrichment culture.** Gas-rich hydrothermally-heated sediments covered with dense mats of *Beggiatoa* were obtained in the Guaymas Basin vent area (27°00.437' N, 11°24.548' W; 2000 m water depth). Samples were collected by push coring using the submersible Alvin (dive 4570) on RV Atlantis during November/December 2009. The sediments were stored anaerobically in butyl rubber stopper-sealed glass vials. In the home laboratory sediments were 1:4 diluted with anoxic artificial seawater (ASW) medium<sup>49</sup>, initially provided with methane as a substrate, and incubated at 50°C. These incubations showed immediate methane-dependent sulfate reduction. After 3 months a subsample was incubated with butane (0.2 MPa). Initially, we did not detect butane-dependent sulfide production, however after 2 months of incubation sulfide production set in. When sulfide concentrations exceeded 15 mM the culture was diluted (1:5) in fresh ASW medium (semi-continuous cultivation) and resupplied with butane. This procedure was repeated several times and resulted in a virtually sediment-free culture after 2 years of cultivation. For quantitative growth experiments, cultures were set up in 150 ml serum bottles containing 80 ml ASW medium, and inoculated with a 20 ml aliquot of a grown culture. Parallel cultures with different starting amounts of butane (5 and 7.5 ml butane in the culture headspace) were prepared. As controls, we used sterile cultures receiving butane, and inoculated cultures lacking butane. All cultures were incubated at 50°C without shaking. Measurements of sulfide production and butane were done in triplicates. **Chemical analyses of sulfide and butane.** Sulfide concentrations were determined by transferring 0.1 ml culture into 4 ml acidified copper sulfate (5 mM) solution. The formation of colloidal copper sulfide was determined photometrically at 480 nm<sup>50</sup>. To quantify butane concentration, volumes of 0.1 ml headspace gas were withdrawn using N<sub>2</sub>-flushed, gas-tight syringes. The gas samples were injected without a split into a Shimadzu GC-14B gas chromatograph, equipped with a Supel-Q PLOT column (30 m × 0.53 mm, 30 μm film thickness; Supelco, Bellefonte, USA) and a flame ionization detector. The oven temperature was maintained at 140°C, and the injection and detection temperatures were maintained at 150°C and 280°C, respectively. The carrier phase was N<sub>2</sub> at a flow rate of 3 ml min<sup>-1</sup>. Samples were analysed in triplicates. Butane concentrations were calculated based on an external calibration curve.

**Detection of autofluorescence in Butane50 culture.** Consortia from the Butane50 culture were visualized by Confocal Laser Scanning Microscopy (LSM 780; Zeiss, Germany) with an excitation light of 405 nm and an emission filter >463 nm, and by recording the maximum autofluorescence at 470 nm wavelength.

**Amplification, sequencing and phylogenetic classification of 16S rRNA and functional genes.** Total DNA was extracted from 10 ml of the Butane50 culture pelleted via centrifugation (4000 rpm for 15 min; Eppendorf Centrifuge 5810R) using the FastDNA Spin Kit for Soil (MP Biomedicals) following the manufacturer's protocols. Bacterial and archaeal 16S rRNA gene fragments were amplified using the primer pairs GM3/GM4<sup>51</sup> and Arch20F<sup>52</sup>/1492R<sup>53</sup>. Furthermore genes encoding canonical anaerobic hydrocarbon-activating enzymes including *assA/masD* (primer pairs 7757F-1, 7757F-2/8543R<sup>54</sup>) and *bssA* (primer pair 1213F/1987R<sup>55</sup>) were targeted for amplification. For amplification of *assA*, a mixture of forward primers was applied to improve diversity coverage<sup>34</sup>. Polymerase chain reactions (PCR) were performed in 20 μl volumes containing 0.5 μM of each primer solution, 7.5/6 μg bovine serum albumin solution, 250 μM deoxynucleoside triphosphate (dNTP) mixture, 1 × PCR reaction buffer (5Prime, Germany), 0.25U Taq DNA polymerase (5Prime) and 1 μl DNA template (25–50 ng). PCR reactions (Mastercycler; Eppendorf) included an initial denaturation step of 95°C for 5 min followed by 34 cycles of denaturation (95°C for 1 min.), annealing (1.5 min at 44°C for bacterial 16S primers, or at 58°C for archaeal 16S primers), and extension (72°C for 3 min) and a final 72°C step for 10 min. For amplification of genes encoding canonical hydrocarbon-activating enzymes, the protocol consisted of an initial denaturation step (95°C for 5 min) followed by 34 cycles of denaturation (96°C for 1 min), annealing (58°C for *assA* primers and 55°C for *bssA* primers, both for 1 min) and extension (72°C for 2 min) ending with a final extension (72°C for 10 min). All products were checked on 1% agarose gels, stained with ethidium bromide and visualized with UV light. Amplicons (archaeal and bacterial 16S rRNA gene) were purified (QIAquick PCR Purification Kit; Qiagen) and cloned in *Escherichia coli* (TOPO TA cloning Kit for sequencing; Invitrogen). Clones were screened by standard PCR procedure and positive inserts were sequenced using Taq cycle sequencing with ABI BigDye Terminator chemistry and an ABI377 sequencer (Applied Biosystems, Foster City, CA, USA). Representative full-length sequences were used for phylogenetic analysis using the ARB software package<sup>56</sup> and the SSURef\_NR99\_115 SILVA database<sup>57</sup>. Phylogenetic trees of 16S rRNA genes were constructed with RAXML (version 7.7.2) using a 50% similarity filter and the GTRGAMMA model. An extended phylogenetic tree is provided as Supplementary Figure 3. Branch support values were determined using 100 bootstrap

replicates. From the Butane50 culture no *masD/assA* and *bssA* genes could be amplified.

**Catalysed reported deposition fluorescence in situ hybridization (CARD-FISH).** Cell aliquots were fixed for 2 hours in 2% formaldehyde, washed and stored in phosphate buffered saline (PBS; pH = 7.4); ethanol 1:1. Samples were sonicated (30 s; Sonoplus HD70; Bandelin) and incubated in 0.1 M HCl (1 min) to remove potential carbonate precipitates. Aliquots were filtered on GTTP polycarbonate filters (0.2 μm pore size; Millipore, Darmstadt, Germany). CARD-FISH was performed according to Pernthaler et al<sup>58</sup> including the following modifications: cells were permeabilised with a lysozyme solution (0.5 M EDTA pH 8.0, 1 M Tris-HCl pH 8.0, 10 mg ml<sup>-1</sup> lysozyme; Sigma-Aldrich) at 37°C for 30 minutes and with a proteinase K solution (0.5 M EDTA, 1 M Tris/HCl, 5 M NaCl, 7.5 μM of proteinase K; Merck, Darmstadt, Germany) for 5 min at room temperature; endogenous peroxidases were inactivated by incubation in a solution of 0.15% H<sub>2</sub>O<sub>2</sub> in methanol for 30 min at room temperature. Specific 16S rRNA-targeting oligonucleotide probes used were SYNA-407 and HotSeep-1-1456<sup>26</sup>, both applied at 20% formamide concentration. SYNA-407 was developed during this project using the probe design tool within the ARB software package to specifically detect *Ca. Syntrophoarchaeum*. The probe is highly specific for *Ca. Syntrophoarchaeum* and has at least one mismatch to non-target group sequences in the current database. The stringency of probe SYNA-407 was experimentally tested on the Butane50 culture using 10% to 40% formamide in the hybridization buffer. The sequence of the probe is: 5' AGTCGACACAGGTGCCGA 3'. Three helpers were necessary: hSYNA-388 (5' ACTCGGAGTCCCCTTATC 3'), hSYNA-369 (5' CACTTGCCTGCATTGTAA 3') and hSYNA-426 (5' TATCCGGACAGTCGACAC 3'). Probes were purchased from Biomers (Ulm, Germany). In case of double hybridization, the peroxidases from the first hybridization were inactivated by incubating the filters in 0.30% H<sub>2</sub>O<sub>2</sub> in methanol for 30 min at room temperature. As fluorochromes Alexa Fluor 488 and Alexa Fluor 594 were used. Finally the filters were stained with DAPI (4',6'-diamino-2-phenylindole) and analysed by epifluorescence microscopy (Axiophot II Imaging, Zeiss, Germany). Selected filters were analysed by Confocal Laser Scanning Microscopy (LSM 780, Zeiss, Germany).

**Extraction of genomic DNA, library construction and sequencing.** Genomic DNA was extracted from 15 ml of the Butane50 culture using the FastDNA Spin Kit for Soil (MP Biomedicals, Illkirch, France). For paired-end library preparation the TruSeq DNA PCR-Free Sample Prep Kit (Illumina) was used including the following modifications of the manufacturer's guidelines: A total amount of 700 ng DNA (in 50 μl volume) was fragmented in 500 μl nebulization buffer (50% glycerol v/v, 35 mM Tris-HCl, 5 mM EDTA), using a Nebulizer (Roche), with a fragmentation time of 3 min, and applied pressure of 32 psi. The fragmented DNA was purified via a MinElute purification column (Qiagen). Following end repair, the first size selection step (removal of large DNA fragments) was done with a sample purification bead/H<sub>2</sub>O mixture of 6/5 (v/v).

For mate-pair library construction, genomic DNA was extracted from 35 ml Butane50 culture following the protocol after Zhou et al<sup>59</sup> with the following modifications: cells were collected by centrifugation of the culture aliquot (3000 × g for 5 min). The pellet was resuspended in 450 μl of extraction buffer, homogenized in a tissue grinder and the mixture was freeze-thawed three times. Subsequently 1350 μl of fresh extraction buffer and 60 μl of Proteinase K were added. In total, 1370 ng of DNA were obtained and used for mate-pair library construction with the Illumina Nextera Mate Pair Sample Preparation Kit following the manufacturer's guidelines with the following modifications: a total amount of 1.3 μg DNA was used and the fragmentation time was reduced to 15 min. Fragments of lengths between 4 kb and 9 kb were obtained on an agarose gel which were then used for further library preparation. Sequencing of both libraries was performed on a MiSeq 2500 instrument (Illumina; 2 × 300 cycles) using v3 sequencing chemistry. In total 4460548 and 21182518 reads were obtained for the paired-end and mate-pair library respectively.

**Read processing, bin assembly and data analysis.** The paired-end Illumina reads were quality-trimmed after adaptor and contaminant removal using the bbdut tool in BBMap (V34: <http://sourceforge.net/projects/bbmap>; minimum quality value of 20; minimum read length ≥ 50 bp). Overlapping paired-end reads were merged using bbmerge when overlap exceeded 20 bases without mismatches for reads ≥ 150 bp. The 16S rRNA based phylogenetic composition of the paired-end library was estimated using the software phyloFlash (<https://github.com/HRGV/phyloFlash>), which classifies reads taxonomically by mapping reads against the SSU SILVA 119 database using bbmap. For quantification, only unambiguously mapped reads were counted. For the mate-pair library, junctions, contaminants and external adaptors were removed using bbdut. Afterwards, the reads were quality trimmed (quality value ≥ 20 and minimum sequence length 50 bp). Bulk assembly of processed libraries was done with SPAdes (version 3.5.0<sup>60</sup>) including the

BayesHammer error correction step and using default k-mer size recommended for the read length (21, 33, 55, 77, 99, 127). The resulting scaffolds were analysed and binned using the Metawatt software (version 2.1<sup>61</sup>), which analyses the GC content, coverage, open reading frames (ORF) and tetranucleotide pattern for each scaffold. The subsequent binning of the scaffolds was based on three different criteria: highly similar tetranucleotide frequency (98% confidence level), coherent taxonomic classification according to BlastP search of the translated ORFs and similar GC content and read coverage in the metagenome. Using the software RNAMmer<sup>62</sup>, the 16S rRNAs present in the bulk assembly were extracted to classify the different bins of the bulk assembly phylogenetically. Bins corresponding to the GoM-Arch87 group were selected and refined. The refinement started with a mapping of the raw reads (from complete libraries) to the selected bins (with a minimum identity of 90% the first time and 97% the next ones) using the bmap tool from the BMap package. The mapped reads were reassembled using SPAdes (same settings as for the bulk assembly), followed by binning in Metawatt. Contigs smaller than 1 kb were removed from the bin. The mate-pair read mapping information of the bin was used to create connectivity graphs using Cytoscape<sup>63,64</sup> and to remove poorly-connected contigs. After bin refinement, its completeness was checked using AMPHORA2<sup>65</sup>, which screens for 104 archaeal single copy genes; CheckM<sup>66</sup>, which analyses completeness and contamination based on lineage-specific marker sets, in our case *Euryarchaeota* and tRNAscan<sup>67</sup>, which screens for the different tRNA sequences. The final bins were used as draft genome of *Ca. S. butanivorans* and *Ca. S. caldarius* for automated gene annotation in RAST<sup>68</sup> and genDB<sup>69</sup> after gene prediction using Glimmer3.02<sup>70</sup>. After selecting the best annotation for each ORF using the automated annotation tool MicHanThi<sup>71</sup>, the GenDB results were visualized using the JCoast frontend<sup>72</sup>. All presented genes were manually curated afterwards.

#### Analysis of species identity and bacterial electron transfer mechanisms.

A HotSeep-1 bin was retrieved and annotated as described above for *Ca. Syntrophoarchaeum*. To compare our HotSeep-1 bin and the published draft genome of *Ca. D. auxilii* (CP013015), JSpecies1.2.1<sup>73</sup> was used, which analyses the average nucleotide identity and the tetranucleotide frequency between two genomes. This method was also used to compare the two genome bins of *Ca. Syntrophoarchaeum*. Furthermore, the two HotSeep-1 strains were compared by checking the identity of the following genes: 16S rRNA, 23S rRNA, sulfate adenyltransferase (*sat*), adenylsulfate reductase subunit alpha (*apr* alpha), adenylsulfate reductase subunit beta (*apr* beta) and dissimilatory sulfite reductase subunit alpha (*dsr* alpha) and of the internal transcribed spacer (ITS) region. To study genes encoding pili and cytochromes of HotSeep-1, genes of interest were identified. This selection was manually curated using Blastp and Pfam search. The subcellular localization of cytochromes was predicted using PSORTb (v.3.0.2<sup>74</sup>).

**Search for canonical alkyl succinate synthase genes.** To search for canonical genes of hydrocarbon oxidation in the metagenome and the bins of *Ca. S. butanivorans* and *Ca. S. caldarius*, a protein database of anaerobic hydrocarbon oxidation genes was constructed. Full-length sequences from hydrocarbon degrading enzymes present in the Uniprot database were combined with recently published *masD* sequences<sup>75</sup>. These enzymes were AssA, BssA, MasD, the alpha subunit from naphthylmethylsuccinate synthase (Nms), the alpha subunit from a ring cleaving hydrolase (BamA), and pyruvate formate lyase (Pfl). The bulk assembly and the *Ca. Syntrophoarchaeum* draft genomes were searched against this database using Blastx with an E-value of 10<sup>-5</sup>.

**Treatment of Butane50 culture with bromoethanesulfonate.** Triplicate Butane50 cultures and duplicates of *Ca. D. auxilii* cultures were grown on their respective substrates (butane or hydrogen). Two active Butane50 cultures were incubated with bromoethanesulfonate (BES, 5 mM final concentration) and as growth control, one culture remained untreated. To check the effect of BES on the bacterial partner alone, hydrogenotrophic grown *Ca. D. auxilii* cultures were also treated with 5 mM of BES. Sulfate-reducing activity was determined by sulfide measurements as described above.

**Phylogenetic analysis of methyl-CoM reductases in *Ca. Syntrophoarchaeum* draft genomes.** The McrA amino acid sequences in the genomes of *Ca. S. butanivorans* and *Ca. S. caldarius* were extracted from the genomic data, and used for a phylogenetic reconstruction. 124 reference McrA protein sequences longer than 450 amino acids from public databases were aligned with Muscle3.7<sup>76</sup>, accession numbers of these sequences are provided in the Supplementary Table 4. After manual refinement of the alignment a masking filter accounting the alignment ambiguity of each column was designed using the ZORRO software<sup>65</sup>. Phylogenetic trees were calculated using Maximum likelihood algorithm RAXML (version 8.2.6<sup>77</sup>) with the masking filter and the PROTGAMMA model with LG as amino acid substitution model and empirical base frequencies. These were the best-fitting conditions according to RAXML using both Akaike and Bayesian information criterion. To find the optimal tree topology 149 bootstraps were calculated

according to the bootstrap convergence criterion of RAXML. To verify results of the presented phylogenetic affiliation, the phylogenetic analyses were repeated using IQ-TREE<sup>78</sup> with LG+I+F+C20 as substitution model on the same alignment (Supplementary Figure 1a).

To avoid the possibility of long branch attraction, further partial McrA sequences of *Bathyarchaeota* (Supplementary Table 4) were included and only the McrA sequence regions common between the partial McrAs of *Bathyarchaeota* and our previous set of full-length sequences (>300 residues) was considered for phylogenetic analysis. First, it was confirmed that using these regions for phylogenetic analysis resulted in similar tree topology as using the full-length sequences by calculating a phylogenetic tree using RAXML (PROTGAMMALG+I+F) with the respective parts of all full-length sequences (the data set used in the previous phylogenetic analysis; Supplementary Figure 1b). Then the partial sequences of *Bathyarchaeota* were included into the set to perform phylogenetic analysis of the common McrA sequence parts using both RAXML (PROTGAMMALG+I+F, Supplementary Figure 1c) and IQ-tree (LG+I+F+C20, Supplementary Figure 1d). Finally, to check if the overall tree topology was influenced by the deeply-branching SCAL\_000352 sequence, a tree using RAXML (PROTGAMMALG+I+F) with only full-length sequences but excluding the SCAL\_000352 sequence was constructed (Supplementary Figure 1e). All resulting trees were plotted using the iTol webserver<sup>79</sup>.

**Verification of different McrA operons.** To test the correct genome assembly and to confirm the presence of four *mcrA* genes per bin, a *mcrA* clone library was constructed. For each of the 8 *mcrA* genes found in the two *Ca. Syntrophoarchaeum* bins primer sets were developed, which were used for PCR amplification from Butane50 culture DNA (Supplementary Table 5). PCR reactions (20 µl volume) were performed containing 1 µM primer each, 200 µM dNTPs, 1 × PCR buffer, and 0.5 U DNA polymerase (TaKaRa Taq, TaKaRa Bio Europe, France) under the following conditions: initial denaturation at 95 °C for 5 min, followed by 39 cycles of denaturation (96 °C, 1 min), annealing for 1 min, elongation (72 °C, 2 min), and a final elongation step (72 °C, 10 min). For two primer sets, amplification was done with Phusion High-Fidelity DNA Polymerase (Thermo Fischer Scientific, Germany) using 50 µl reactions containing 1.5 mM MgCl<sub>2</sub>, 3% (v/v) DMSO, 0.4 µM primer each, 50 µM dNTPs, 1 × PCR buffer, and 1 U DNA polymerase under the following conditions: initial denaturation at 98 °C for 30 s, followed by 39 cycles of denaturation (98 °C, 10 s), annealing for 30 s, elongation (72 °C, 50 s), and a final elongation step (72 °C, 10 min). For annealing temperatures for the individual primer sets see Supplementary Table 5. PCR resulted in multiple bands, therefore amplicons of expected size were excised from an 1% agarose gel and purified using the MinElute Gel extraction kit (Qiagen, Germany). DNA was ligated in a pGEM T-Easy vector (Promega, Madison, WI) and transformed into *E. coli* TOP10 cells (Invitrogen, Carlsbad, CA) according to the manufacturers' recommendations. Sequencing was performed by Taq cycle sequencing using a vector-specific primer (M13F or M13R) with a model ABI377 sequencer (Applied Biosystems). Sequence data were analysed with the ARB software package<sup>80</sup>.

**Extraction of RNA, library construction and data analysis.** Total RNA was extracted from 100 ml of an active Butane50 culture, which was kept at 50 °C during the whole procedure: first most medium (>90%) was replaced by butane gas, whereas the biomass remained at the bottom of the bottle. Then RNA was preserved by adding 90 ml preheated RNAlater (Sigma-Aldrich; 10:1 RNAlater vs. sample) for 1 hour. Subsequently this mixture was filtered through an RNA-free cellulose nitrate filter (pore size 0.45 µm; Sartorius; Göttingen, Germany). The filter was extracted in an RNase-free tube with glass beads and 600 µl of RNA Lysis Buffer (Quick-RNA MiniPrep, Zymoresearch, USA) applying bead beating (2 cycles of 6 m/s for 20 s). The lysate was cleared by centrifugation (10000g; 1 min) and the supernatant was used for RNA extraction with the Quick-RNA MiniPrep Kit (Zymoresearch, Irvine, CA, USA) according to the manufacturer's guidelines but omitting the on-column DNase treatment step. The RNA extract was cleaned from DNA by incubating it at 37 °C for 40 min with 10 µl of DNase I (DNase I recombinant, RNA-free; Roche Diagnostics, Mannheim, Germany), 7 µl of 10 × incubation buffer (Roche) and 2 µl of RNase-Inhibitor (Protector RNase Inhibitor, Roche Diagnostics, Mannheim, Germany). DNases were inactivated by heating for 10 min to 56 °C. Subsequently the RNA was purified with the RNeasy MinElute Cleanup Kit (QIAGEN, Hilden, Germany). In total 450 ng high quality RNA were obtained.

The TruSeq Stranded Total RNA Kit (Illumina) was used for RNA library preparation. The rRNA depletion step was omitted. 80 ng of the total RNA (in 5 µl volume) was combined with 13 µl of 'Fragment, Prime and Finish mix', for the RNA fragmentation step according to the Illumina TruSeq stranded mRNA sample preparation guide. Subsequent steps were performed as described in the sample preparation guide. The library was sequenced on a MiSeq instrument; with v3 sequencing chemistry in 2 × 75 cycles paired-end runs. The resulting reads

were pre-processed including removal of adaptors and contaminants and quality trimming to Q10 using bbdduk v34 from the BMAP package. Trimmed reads were used to quantify the 16S rRNA gene based phylogenetic composition of the library by phyloFlash as described above for the DNA paired-end library. Trimmed reads were also mapped to the bins of interest (*Ca. S. butanivorans*, HotSeep-1) using bmap with a minimum identity of 97%. The expression level of each gene was quantified by counting the number of unambiguously mapped reads per gene using featureCount<sup>80</sup> with the  $-p$  option to count fragments instead of reads. To compare expression levels between genes, absolute fragment counts per genes were converted into Fragments Per Kilobase of transcript per Million mapped reads (FPKM<sup>81</sup>) as follows:

$$FPKM_i = \frac{C_i}{L_i \sum_j C_j} \times 10^9$$

where  $i$  = any specific gene,  $j$  = sum of all the transcribed genes,  $C$  = counts and  $L$  = length (bp).

**Protein analysis by nanoLC-MS/MS.** For total protein analysis, the cells from 50 ml of grown (ca. 10 mM sulfide) Butane50 enrichment culture were harvested by centrifugation, frozen in liquid nitrogen and stored at  $-20^\circ\text{C}$  until analysis. The cell pellets were suspended in  $30\ \mu\text{l}$  of 50 mM ammonium bicarbonate buffer, and lysed by three 60 s freeze-thaw cycles between liquid nitrogen and  $+40^\circ\text{C}$  (thermal shaker, 1400 rpm). The cell lysate was incubated with 50 mM dithiothreitol at  $30^\circ\text{C}$  for 1 h, followed by alkylation with 200 mM iodoacetamide for 1 h at room temperature, in the dark, and trypsin digestion (0.6  $\mu\text{g}$  trypsin, Promega) overnight at  $37^\circ\text{C}$ . Peptides were desalted using C18 Zip Tip columns (Millipore), and analysed by nLC-MS/MS using an LTQ-Orbitrap mass spectrometer (Thermo Fisher Scientific) equipped with a nanoUPLC system (nanoAquty, Waters) as described before<sup>82</sup>.

Peptide identification was conducted by Proteome Discoverer (v1.4.1.14, Thermo Fisher Scientific) using the Mascot search engine with the annotated metagenome of *Ca. Syntrophoarchaeum* as database<sup>82</sup>. Peptides were considered to be identified by Mascot when a probability of 0.05 (probability-based ion score threshold of 40) was achieved. emPAI values calculated by Mascot for identified proteins were used as semi-quantitative measure to estimate the abundance of proteins in the analysed sample<sup>83</sup>. The mass spectrometry proteomics data have been deposited to the ProteomeXchange Consortium<sup>84</sup> via the PRIDE partner repository<sup>85</sup>.

**Synthesis of authentic standards.** To synthesize 1-butyl-CoM and 2-butyl-CoM, 5 g of coenzyme M (Na 2-mercaptoethanesulfonate, purity 98%; Sigma Aldrich) were dissolved in 40 ml of a 30% (v/v) ammonium hydroxide solution, in serum vials. Twice the molar amount of 1-bromobutane (purity 99%; Sigma Aldrich) or 2-bromobutane (purity 98%; Sigma Aldrich) were added, the serum bottles were closed with butyl rubber septa and incubated at room temperature with vigorous shaking (500 rpm) for 4 h. The aqueous phase was separated from the excess hydrophobic 1- or 2-bromobutane via separatory funnels. Residual, dissolved 1- or 2-bromobutane was removed by bubbling with nitrogen. The solutions were analysed for the presence of 1-butyl-CoM or 2-butyl-CoM by FT-ICR-MS analysis without further purification. Both solutions contained a major  $m/z$  peak at 197.0311; no  $m/z$  peaks indicative of free CoM, CoM dimers, 1- or 2-bromobutane were detected. Both standards were stable and no interconversion of isomers was observed.

**Metabolite extraction.** For preparation of cell extracts, volumes of 20 ml were collected from grown Butane50 cultures (sulfide concentrations of 14–15 mM) under anoxic conditions. The cells were harvested by centrifugation (10 min, 10,000 rpm,  $4^\circ\text{C}$ ), washed twice with a 100 mM ammonium bicarbonate solution, and finally suspended in 1 ml of acetonitrile: methanol: water solution (40:40:20 v/v). Glass beads (0.1 mm diameter, Roth) were added (0.3 g per tube), and the cells were lysed with a PowerLyzer 24 bench top bead-based homogenizer (MO BIO Laboratories, Carlsbad, CA) using 5 cycles of 2000 rpm for 50 sec, with a 15 sec pause between cycles. Prior use, the glass beads were treated with 1N HCl solution and washed twice with deionized water. Glass beads and cell debris were removed by centrifugation, and the aqueous cell extracts were stored in glass vials at  $4^\circ\text{C}$  until analysis.

**Mass spectrometry of cell extracts and standards.** Authentic standards and cell extract samples were measured with ultra-high resolution mass spectrometry (Solarix XR 12T Fourier transform ion cyclotron resonance mass spectrometer, Bruker Daltonics Inc., Billerica, MA) with negative electrospray ionization (capillary voltage: 4.5 kV) in direct infusion mode ( $4\ \mu\text{l}/\text{min}$  and 0.1 s accumulation time). Spectra were recorded with a 2 MWord time domain (0.42 s transient length) between  $m/z$  74 and 3000 resulting in a mass resolution of ca. 250,000 at  $m/z$  200. Instrument mass accuracy was linearly calibrated with low-molecular mass fatty acids (C4 - C12) between 88 and 199 Da, resulting in an average root-mean square error of the calibration masses of 39 ppb ( $n = 7$ ). For each measurement, 64 (Butane50 samples), or 128 (controls) spectra were co-added (lock mass: 143.10775  $m/z$ ) and internally recalibrated with naturally present fatty acids.

Collision induced fragmentation of  $m/z$  197 was carried out after quadrupole isolation (10 Da window) with 12 V collision energy and 128 scans per measurement (lock mass: 199.17035  $m/z$ ). The 1-butyl-CoM and 2-butyl-CoM standards were diluted to ca. 10  $\mu\text{g}/\text{ml}$  and checked for appropriate collision energy and fragment pattern. Fragment masses 89.0430 ( $\text{C}_4\text{H}_9\text{S}^-$ ) and 80.9652 ( $\text{HSO}_3^-$ ) were then used as indicative fragment for butyl-CoM in the cell extracts. The formation of an even-electron fragment  $\text{HSO}_3^-$  from bisulfite is favoured when a  $\beta$ -H-atom is present<sup>86</sup>. However,  $\text{SO}_3^-$  ( $m/z = 79.9674$ ) was also produced upon fragmentation of the standards.

Fragmentation information of the butyl-CoM standards was used to implement a UPLC-MS/MS method to validate the isomeric form of  $m/z$  197.031 in the samples. A triple quadrupole mass spectrometer (Xevo TQ-S, Waters Cooperation, Manchester, UK) in negative electrospray ionization mode was used in multiple reaction monitoring (MRM) mode. Indicative butyl-CoM transitions ( $m/z$  197 > 89 and  $m/z$  197 > 81) were initially optimized (cone voltage and collision energy) by direct infusion of standard solutions into the mass spectrometer. The mass spectrometer was coupled to a UPLC (ACQUITY I-Class, Waters Cooperation Milford, MA, USA) equipped with a reversed phase column (HSS T3, 25 cm, Waters) and run with a binary gradient (1% methanol in Water to 90% methanol) at a flow rate of  $0.3\ \text{ml}\ \text{min}^{-1}$ . For each analysis,  $10\ \mu\text{l}$  were injected into the UPLC. Retention time, presence of both MRM transitions and relative ion ratios as compared to the standards were used as quality criteria.

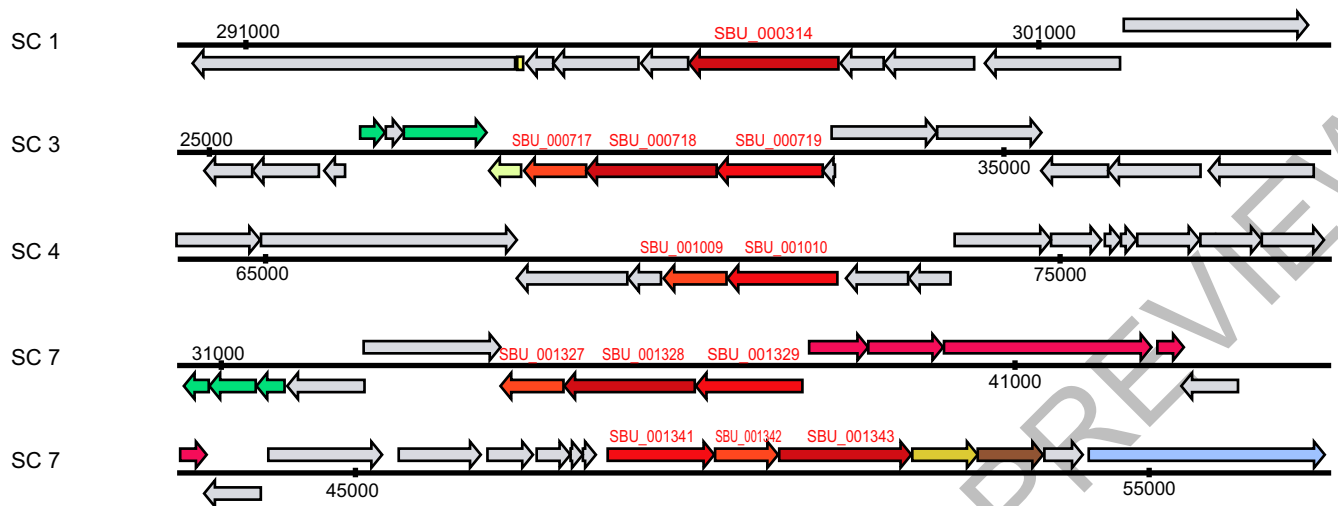
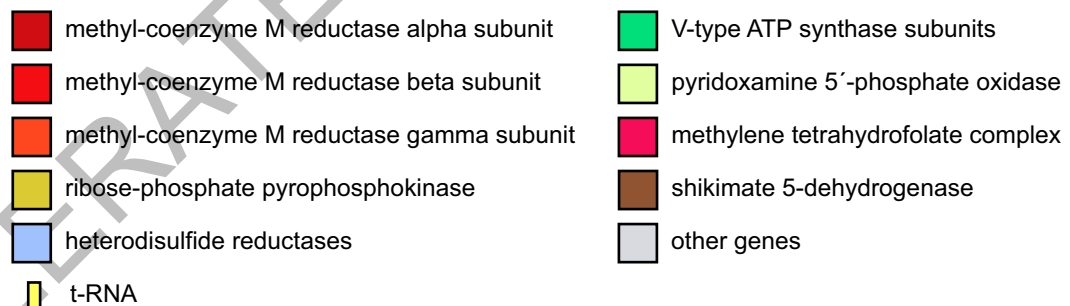
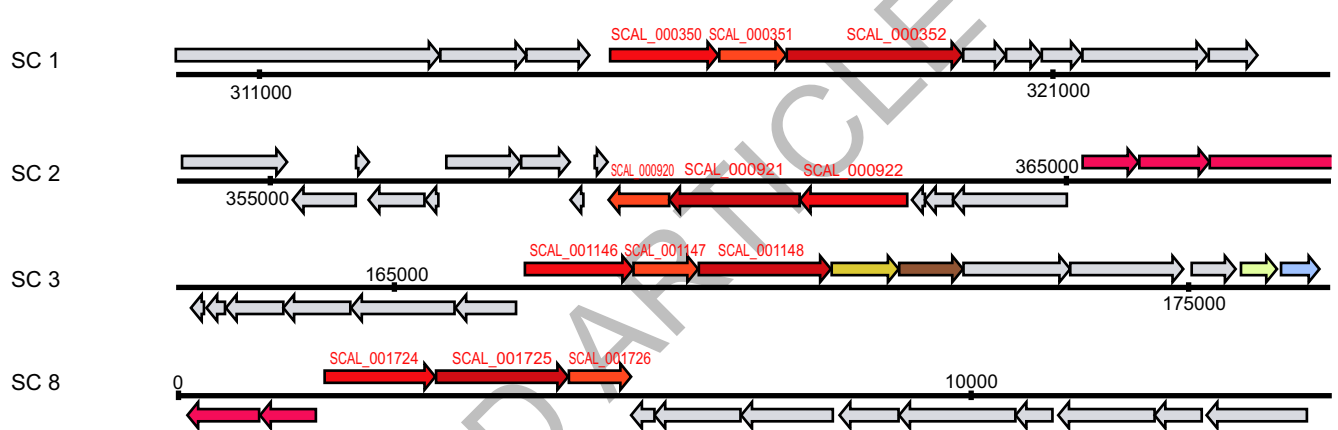
**Quantification of hydrogen production in experiment.** Hydrogen production in the Butane50 culture was measured by analysing the headspace of replicate incubations which were constantly agitated on a shaking table in a  $50^\circ\text{C}$ -incubator. The butane-dependent sulfide production (and therefore potential hydrogen production) was determined from tracking the sulfide production (as above) for 4 weeks. Gas phase (1 ml) was sampled with a gas-tight syringe to determine hydrogen concentrations (i) before changing the headspace, (ii) after exchanging the headspace in 30 minute intervals for 6 hours (iii) the next day, before and after addition of sodium molybdate solution (10 mM final concentration) to the culture to stop potential hydrogen-dependent sulfate reduction. Gas phase was immediately injected into a Peak Performer 1 gas chromatograph (Peak Laboratories, Palo Alto, CA) equipped with a reducing compound photometer. Development of hydrogen concentrations were converted into hydrogen production rates and compared with potential hydrogen production rates according to a stoichiometry of 4:1 ( $\text{H}_2$ -production vs. sulfate reduction).

**Transmission electron microscopy.** A 100 ml grown Butane50 culture was concentrated by centrifugation at 2,000 rpm using a Stat Spin Microprep 2 table-top centrifuge. Aliquots were placed in aluminium platelets of 150  $\mu\text{m}$  depth containing 1-hexadecen<sup>87</sup>. The platelets were frozen using a Leica EM HPM100 high pressure freezer (Leica Mikrosysteme, Wetzlar, Germany). The frozen samples were transferred to an Automatic Freeze Substitution Unit (Leica EM AFS2) and substituted at  $-90^\circ\text{C}$  in a solution containing anhydrous acetone, 0.1% tannic acid for 24 h and in anhydrous acetone, 2%  $\text{OsO}_4$ , 0.5% anhydrous glutaraldehyde (Electron Microscopy Sciences, Ft. Washington, USA) for additional 8 h. After a further incubation over 20 h at  $-20^\circ\text{C}$  samples were warmed up to  $+4^\circ\text{C}$  and washed with anhydrous acetone subsequently. The samples were embedded at room temperature in Agar 100 (Epon 812 equivalent) at  $60^\circ\text{C}$  over 24 h. Thin sections (80 nm) were examined using a Philips CM 120 BioTwin transmission electron microscope (Philips Inc. Eindhoven, The Netherlands). Images were recorded with a TemCam F416 CMOS camera (TVIPS, Gauting, Germany), for additional images see Supplementary Figure 4.

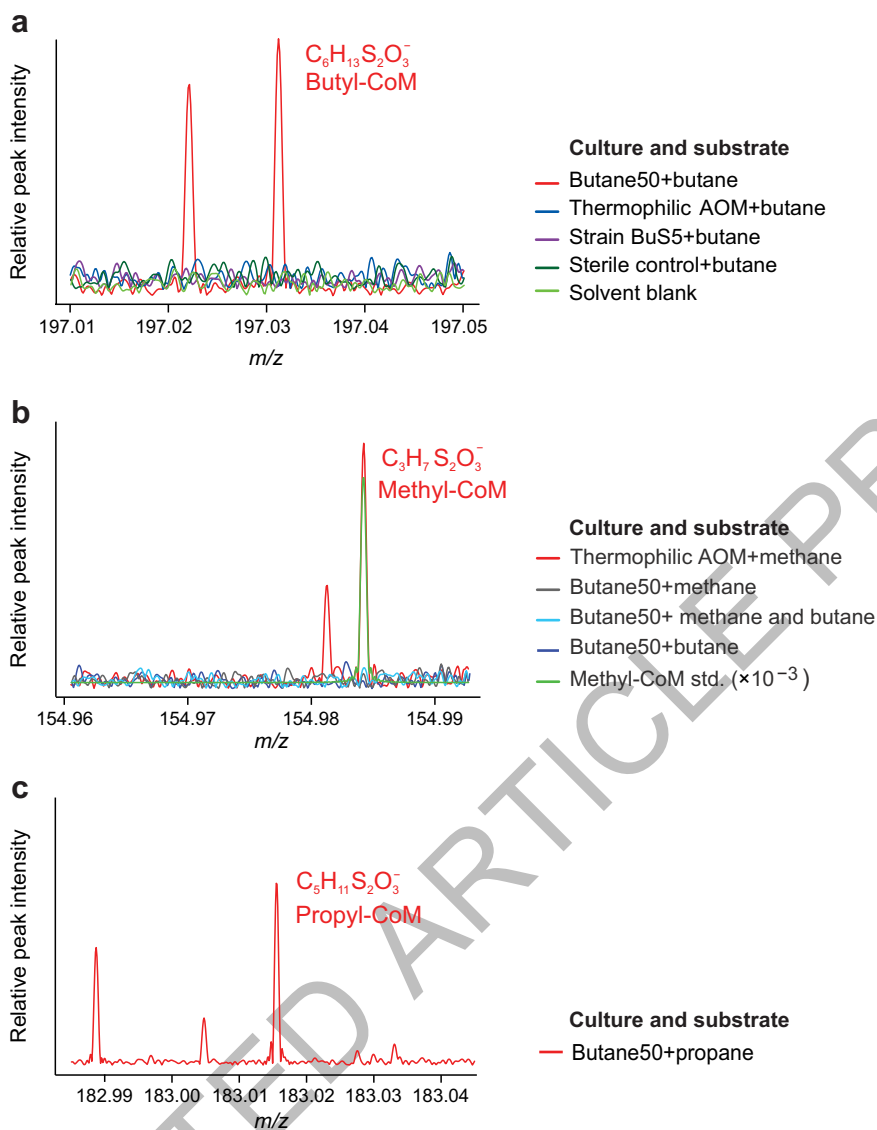
**Data availability.** All sequence data are archived in NCBI database under the BioSample number SAMN05004607. Representative full-length 16S rRNA gene sequences of the clone library of the Butane50 culture have been submitted to NCBI under accession numbers KX812780-KX812802. Draft genomes of the *Ca. Syntrophoarchaeum* organisms can be found under the BioProject PRJNA318983 (*Ca. S. butanivorans*) and PRJNA319143 (*Ca. S. caldarius*). Metagenomic and metatranscriptomic reads have been submitted to the short read archive SRS1505411. The mass spectra of the proteomic dataset have been deposited to the ProteomeXchange Consortium with the dataset identifier PXD005038.

49. Widdel, F. & Bak, F. In *The prokaryotes* Vol. 4 (ed Trüper HG Balows A, Dworkin M, Harder W, Schleifer KH) 3352–3378 (Springer, 1992).
50. Cord-Ruwisch, R. A quick method for the determination of dissolved and precipitated sulfides in cultures of sulfate-reducing bacteria. *Microbiol Meth* **4**, 33–36 (1985).
51. Muyzer, G., Teske, A., Wirsén, C. O. & Jannasch, H. W. Phylogenetic relationships of *Thiomicrospira* species and their identification in deep-sea hydrothermal vent samples by denaturing gradient gel electrophoresis of 16S rDNA fragments. *Arch Microbiol* **164**, 165–172 (1995).
52. Massana, R., Murray, A. E., Preston, C. M. & DeLong, E. F. Vertical distribution and phylogenetic characterization of marine planktonic Archaea in the Santa Barbara Channel. *Applied and environmental microbiology* **63**, 50–56 (1997).

53. Teske, A. *et al.* Microbial diversity of hydrothermal sediments in the Guaymas Basin: evidence for anaerobic methanotrophic communities. *Applied and environmental microbiology* **68**, 1994–2007 (2002).
54. von Netzer, F. *et al.* Enhanced gene detection assays for fumarate-adding enzymes allow uncovering of anaerobic hydrocarbon degraders in terrestrial and marine systems. *Appl. Environ. Microbiol.* **79**, 543–552 (2013).
55. Callaghan, A. V. *et al.* Diversity of benzyl- and alkylsuccinate synthase genes in hydrocarbon-impacted environments and enrichment cultures. *Environmental science & technology* **44**, 7287–7294 (2010).
56. Ludwig, W. *et al.* ARB: a software environment for sequence data. *Nucleic Acids Research* **32**, 1363–1371, doi:10.1093/nar/gkh293 (2004).
57. Quast, C. *et al.* The SILVA ribosomal RNA gene database project: improved data processing and web-based tools. *Nucleic Acids Research* **41**, D590–596, doi:10.1093/nar/gks1219 (2013).
58. Pernthaler, A., Pernthaler, J. & Amann, R. Fluorescence in situ hybridization and catalyzed reporter deposition for the identification of marine bacteria. *Applied and environmental microbiology* **68**, 3094–3101 (2002).
59. Zhou, J., Bruns, M. A. & Tiedje, J. M. DNA recovery from soils of diverse composition. *Applied and environmental microbiology* **62**, 316–322 (1996).
60. Bankevich, A. *et al.* SPAdes: a new genome assembly algorithm and its applications to single-cell sequencing. *Journal of Computational Biology* **19**, 455–477 (2012).
61. Strous, M., Kraft, B., Bisdorf, R. & Tegetmeyer, H. E. The binning of metagenomic contigs for microbial physiology of mixed cultures. *Front. Microbiol.* **3**, 410, doi:10.3389/fmicb.2012.00410 (2012).
62. Lagesen, K. *et al.* RNAmmer: consistent and rapid annotation of ribosomal RNA genes. *Nucleic acids research* **35**, 3100–3108 (2007).
63. Shannon, P. *et al.* Cytoscape: a software environment for integrated models of biomolecular interaction networks. *Genome Res.* **13**, 2498–2504 (2003).
64. Albertsen, M. *et al.* Genome sequences of rare, uncultured bacteria obtained by differential coverage binning of multiple metagenomes. *Nature biotechnology* **31**, 533–538 (2013).
65. Wu, M. & Scott, A. J. Phylogenomic analysis of bacterial and archaeal sequences with AMPHORA2. *Bioinformatics* **28**, 1033–1034 (2012).
66. Parks, D. H., Imelfort, M., Skennerton, C. T., Hugenholtz, P. & Tyson, G. W. CheckM: assessing the quality of microbial genomes recovered from isolates, single cells, and metagenomes. Report No. 2167-9843, (PeerJ PrePrints, 2014).
67. Schattner, P., Brooks, A. N. & Lowe, T. M. The tRNAscan-SE, snoscan and snoGPS web servers for the detection of tRNAs and snoRNAs. *Nucleic acids research* **33**, W686–W689 (2005).
68. Aziz, R. K. *et al.* The RAST Server: rapid annotations using subsystems technology. *BMC genomics* **9**, 75 (2008).
69. Meyer, F. *et al.* GenDB - an open source genome annotation system for prokaryote genomes. *Nucleic acids research* **31**, 2187–2195, doi:10.1093/nar/gkg312 (2003).
70. Delcher, A. L., Bratke, K. A., Powers, E. C. & Salzberg, S. L. Identifying bacterial genes and endosymbiont DNA with Glimmer. *Bioinformatics* **23**, 673–679 (2007).
71. Quast, C. MicHanThi-design and implementation of a system for the prediction of gene functions in genome annotation projects. *Universität Bremen, Diploma work* (2006).
72. Richter, M. *et al.* JCoast-A biologist-centric software tool for data mining and comparison of prokaryotic (meta) genomes. *BMC bioinformatics* **9**, 177 (2008).
73. Richter, M. & Rossello-Mora, R. Shifting the genomic gold standard for the prokaryotic species definition. *Proc. Natl. Acad. Sci. USA* **106**, 19126–19131, doi:10.1073/pnas.0906412106 (2009).
74. Yu, N. Y. *et al.* PSORTb 3.0: improved protein subcellular localization prediction with refined localization subcategories and predictive capabilities for all prokaryotes. *Bioinformatics* **26**, 1608–1615, doi:10.1093/bioinformatics/btq249 (2010).
75. Stagars, M. H., Ruff, S. E., Amann, R. & Knittel, K. High diversity of anaerobic alkane-degrading microbial communities in marine seep sediments based on (1-methylalkyl)succinate synthase genes. *Frontiers in Microbiology* **6**, doi:10.3389/fmicb.2015.01511 (2016).
76. Edgar, R. C. MUSCLE: multiple sequence alignment with high accuracy and high throughput. *Nucleic acids research* **32**, 1792–1797 (2004).
77. Stamatakis, A. RAxML-VI-HPC: maximum likelihood-based phylogenetic analyses with thousands of taxa and mixed models. *Bioinformatics* **22**, 2688–2690 (2006).
78. Letunic, I. & Bork, P. Interactive Tree Of Life (iTOL): an online tool for phylogenetic tree display and annotation. *Bioinformatics* **23**, 127–128 (2007).
79. Nguyen, L.-T., Schmidt, H. A., von Haeseler, A. & Minh, B. Q. IQ-TREE: A Fast and Effective Stochastic Algorithm for Estimating Maximum-Likelihood Phylogenies. *Mol. Biol. Evol.* **32**, 268–274, doi:10.1093/molbev/msu300 (2015).
80. Liao, Y., Smyth, G. & Shi, W. featureCounts: an efficient general-purpose read summarization program. *arXiv* **1305**, 16 (2013).
81. Mortazavi, A., Williams, B. A., McCue, K., Schaeffer, L. & Wold, B. Mapping and quantifying mammalian transcriptomes by RNA-Seq. *Nat. Meth.* **5**, 621–628 (2008).
82. Wagner, A., Cooper, M., Ferdi, S., Seifert, J. & Adrian, L. Growth of *Dehalococcoides mccartyi* strain CBDB1 by reductive dehalogenation of brominated benzenes to benzene. *Environmental science & technology* **46**, 8960–8968, doi:10.1021/es3003519 (2012).
83. Ishihama, Y. *et al.* Exponentially Modified Protein Abundance Index (emPAI) for Estimation of Absolute Protein Amount in Proteomics by the Number of Sequenced Peptides per Protein. *Molecular & Cellular Proteomics* **4**, 1265–1272, doi:10.1074/mcp.M500061-MCP200 (2005).
84. Vizcaino, J. A. *et al.* ProteomeXchange provides globally coordinated proteomics data submission and dissemination. *Nat Biotech* **32**, 223–226, doi:10.1038/nbt.2839 (2008).
85. Vizcaino, J. A. *et al.* 2016 update of the PRIDE database and its related tools. *Nucleic acids research* **44**, D447–D456, doi:10.1093/nar/gkv1145 (2016).
86. Jariwala, F. B., Wood, R. E., Nishshanka, U. & Attygalle, A. B. Formation of the bisulfite anion (HSO<sub>3</sub><sup>-</sup>, m/z 81) upon collision induced dissociation of anions derived from organic sulfonic acids. *Journal of Mass Spectrometry* **47**, 529–538 (2012).
87. Studer, D., Michel, M. & Müller, M. High pressure freezing comes of age. *Scanning microscopy* **3**, 253–268 (1988).

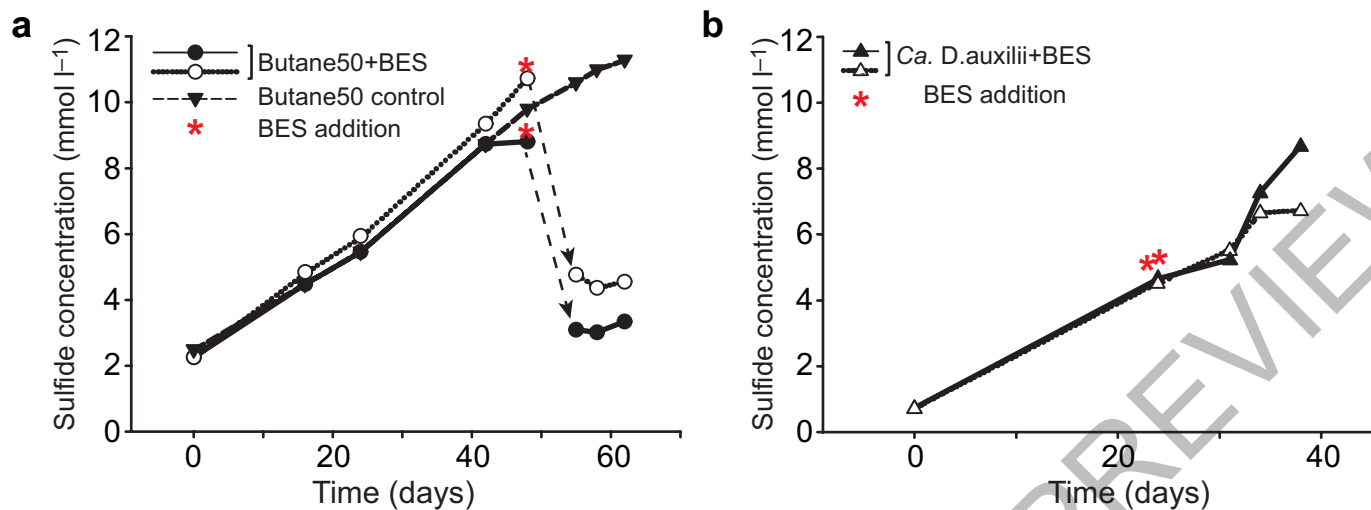
**Ca. S. butanivorans (SBU)****Ca. S. caldarius (SCAL)**

Extended Data Figure 1 | Genetic structure of *mcr* genes in *Ca. Syntrophoarchaeum*. In *Ca. S. butanivorans* one *mcr* gene set is separated, with the *mcrA* subunit in scaffold 1, and *mcrB* and *mcrG* in scaffold 4.



**Extended Data Figure 2 | Experiments validating production of alkyl-CoM compounds in anaerobic cultures.** **a**, Screening for butyl-CoM in Butane50, in a thermophilic AOM culture supplied with butane ( $n = 2$  with 2 different sampling time points), in BuS5 cultures ( $n = 3$ ) and in controls. The mass peak of butyl-CoM ( $m/z = 197.0312$ ) was only found in the Butane50 culture. **b**, Screening for methyl-CoM ( $m/z = 154.984$ ; mass accuracy  $-0.15$  ppm) in the thermophilic AOM culture supplied with

methane ( $n = 3$ ) and in the Butane50 culture ( $n = 2$ ). Methyl-CoM was only found in the thermophilic AOM culture. These analyses (**a**,**b**) indicate high substrate specificity of the organisms in the two different cultures. **c**, The also established propane-degrading culture ( $n = 1$ ) forms propyl-CoM ( $m/z = 183.016$ ; mass accuracy  $-0.21$  ppm) showing CoM-type activation of this substrate.



**Extended Data Figure 3 | Effect of bromoethanesulfonate (BES) on Butane50 and *Ca. D. auxilii* cultures.** After growth on their specific substrates, BES (5 mM final concentration) was added to **a**, Butane50 cultures (circles,  $n = 2$ ) where it immediately inhibited butane-dependent

sulfate reduction compared to a control without BES (triangles,  $n = 1$ ) and to **b**, *Ca. D. auxilii* cultures (triangles,  $n = 2$ ) where it had no influence on hydrogen-dependent sulfate reduction.

Extended Data Table 1 | Microbial diversity in the early AOM enrichment<sup>21</sup> used as inoculum and in the Butane50 culture

Phylogenetic group	Early AOM enrichment		Butane50 culture*	
	Clones	Clones	Metagenome reads	Metatranscriptome reads
<b>Archaea</b>				
<i>Euryarchaeota</i>				
<i>Methanomicrobia</i>				
GoM-Arch87		46	596	32009
<i>Methermicoccus</i>				2316
ANME-1	46			1465
<i>Thermoplasmata</i>	6			
19c-33 cluster		38	199	
pMC2A24 cluster		1	30	
20c-4 cluster			132	
<i>Halobacteria</i>	4			
<b>Sum</b>	<b>56</b>	<b>85</b>	<b>957</b>	<b>35790</b>
<b>Bacteria</b>				
<i>Proteobacteria</i>				
<i>Deltaproteobacteria</i>				
HotSeep-1 cluster	53	63	575	4780
<i>Syntrophobacteraceae</i>	1	5		626
Others	3	3		
<i>Spirochaete</i>				
Kazan-3B-09		1		
TA06		8	44	
Candidate division OP3	3	6	36	
Candidate division KB1			159	827
Candidate division WS3			33	
BHI80-139		1		
<i>Chloroflexi</i>	3			
<i>Anaerolineaceae</i>		3	138	
Others	17			
<b>Sum</b>	<b>80</b>	<b>92</b>	<b>985</b>	<b>6233</b>

\*based on 16S rRNA gene sequences retrieved by clone library approach from the Butane50 culture, and found in the metagenome and metatranscriptome libraries using the phyloFlash software. Taxa which account for  $\geq 1\%$  of all 16S rRNA gene sequences are shown.

Extended Data Table 2 | Draft genome information and pairwise comparison of whole genome identity of *Ca. S. butanivorans* and the *Ca. S. caldarius*

	<i>Candidatus</i> Syntrophoarchaeum butanivorans	<i>Candidatus</i> Syntrophoarchaeum caldarius	
Size (base pair)	1,456,963	1,666,081	
Scaffolds/Contigs	16/21	10/15	
Scaffold N50 (bp)	219,218	410,601	
Coverage (times)	360	134	
GC content (%)	48.7	45.5	
Number of ORFs	1,604	1,790	
rRNAs	3	3	
tRNAs	39	44	
Genome Completeness (%)	85 <sup>1</sup> ; 88 <sup>2</sup> ; 89 <sup>3</sup>	95 <sup>1</sup> ; 97 <sup>2</sup> ; 96 <sup>3</sup>	
Contamination <sup>3</sup> (%)	0.97	0.32	
Duplication of single copy genes <sup>3</sup>	2	1	
Strain heterogeneity <sup>3</sup> (%)	0	0	
	Average Nucleotide Identity (Blast)	Average Nucleotide Identity (MUMmer)	Tetranucleotide frequency
<i>Ca. S. butanivorans</i> / <i>Ca. S.</i> <i>caldarius</i>	73.57	89.57	88.19
<i>Ca. S. caldarius</i> / <i>Ca. S.</i> <i>butanivorans</i>	73.56	89.03	88.19

<sup>1</sup>Based on tRNA completeness, using tRNAscan;<sup>2</sup>based on archaea-specific single copy genes, using AMPHORA2; <sup>3</sup>based on lineage-specific marker genes of *Euryarchaeota*, using CheckM

Extended Data Table 3 | Genes encoding enzymes for butane activation, candidates for further conversion reactions and butyryl-CoA oxidation in *Ca. S. butanivorans*

Gene	Feature	Locus tag	Transcriptome		Proteome
			Absolute reads	FPKM	emPAI
<b>Butane activation</b>					
<i>mcrA</i>	Methyl coenzyme M reductase alpha	SBU_000314	8320	491.4	0.15
<i>mcrA</i>	Methyl coenzyme M reductase alpha	SBU_000718	1640	108.9	0.05
<i>mcrA</i>	Methyl coenzyme M reductase alpha	SBU_001328	514	34.13	
<i>mcrA</i>	Methyl coenzyme M reductase alpha	SBU_001343	1077	70.5	0.11
<i>mcrB</i>	Methyl coenzyme M reductase beta	SBU_000719	5047	418.0	0.07
<i>mcrB</i>	Methyl coenzyme M reductase beta	SBU_001010	2628	210.1	0.46
<i>mcrB</i>	Methyl coenzyme M reductase beta	SBU_001329	311	25.7	
<i>mcrB</i>	Methyl coenzyme M reductase beta	SBU_001341	602	49.0	0.3
<i>mcrG</i>	Methyl coenzyme M reductase gamma	SBU_000717	689	97.7	
<i>mcrG</i>	Methyl coenzyme M reductase gamma	SBU_001009	1787	243.0	0.5
<i>mcrG</i>	Methyl coenzyme M reductase gamma	SBU_001327	642	91.4	
<i>mcrG</i>	Methyl coenzyme M reductase gamma	SBU_001342	366	52.3	0.37
<i>hdrA</i>	CoB--CoM heterodisulphide reductase,	SBU_000296	2586	94.9	0.12
<i>hdrB</i>	CoB--CoM heterodisulphide reductase,	SBU_000294	222	27.4	
<i>hdrC</i>	CoB--CoM heterodisulphide reductase,	SBU_000295	127	36.3	0.35
<i>hdrA</i>	Heterodisulfide reductase subunit A	SBU_001347	459	16.9	
<i>hdrA</i>	Heterodisulfide reductase subunit A	SBU_001502	903	60.7	0.05
<i>hdrA</i>	Heterodisulfide reductase subunit A	SBU_001503	995	56.9	0.14
<b>Candidates for conversion to butyryl-CoA</b>					
<i>mtaA</i>	Methyltransferase corrinoid activation protein	SBU_000376	1503	83.6	0.36
<i>mtaA</i>	Methylcobamide:CoM methyltransferase	SBU_000378	583	61.7	0.09
<i>mtaA</i>	Methylcobamide:CoM methyltransferase	SBU_000450	988	101.7	0.61
<i>mtaA</i>	Methylcobamide:CoM methyltransferase	SBU_001175	274	28.4	
<i>mtaA</i>	Methylcobamide:CoM methyltransferase	SBU_001379	133	13.6	
<i>mtaA</i>	Methylcobamide:CoM methyltransferase	SBU_001480	553	57.7	0.08
<i>mtaC</i>	Corrinoid protein	SBU_000377	1016	156.7	1.33
<i>mtaC</i>	Corrinoid methyltransferase	SBU_001174	95	16.0	
<b>Butyryl-CoA oxidation</b>					
	Acyl-CoA dehydrogenase domain-containing	SBU_000172	1751	168.5	1.43
	Acyl-CoA dehydrogenase	SBU_000399	2844	205.1	0.55
	Acyl-CoA dehydrogenase domain-containing	SBU_000724	449	42.9	0.25
	Acyl-CoA dehydrogenase	SBU_001146	177	12.4	0.11
<i>crt</i>	Crotonase	SBU_000400	1745	236.4	1.65
	3-Hydroxyacyl-CoA dehydrogenase	SBU_000288	2425	312.5	0.81
	3-Hydroxyacyl-CoA dehydrogenase	SBU_000843	1151	162.5	0.12
	Acetyl-CoA acetyltransferase	SBU_000329	103	9.8	
	Acetyl-CoA acetyltransferase	SBU_000402	3198	295.4	0.34
	Acetyl-CoA acetyltransferase	SBU_000404	1644	152.6	0.16
	Acetyl-CoA acetyltransferase	SBU_001291	161	15.5	
<i>etfA</i>	Electron transfer flavoprotein subunit alpha	SBU_000173	557	63.6	0.1
<i>etfB</i>	Electron transfer flavoprotein subunit beta	SBU_000174	506	69.8	0.58
	Fe-S Oxidoreductase	SBU_000175	402	38.8	0.55

Expression as absolute read counts and as fragments per kilobase of transcript per million mapped reads (FPKM) is shown, as well as the corresponding protein abundance as emPAI index.

Extended Data Table 4 | Genes encoding enzymes of C-1 pathway in *Ca. S. butanivorans*

Gene	Feature	Locus_tag	Transcriptome		Proteome
			Absolute reads	FPKM	emPAI
<i>cdhA</i>	Acetyl-CoA decarboxylase/synthase complex alpha	SBU_000891	3756	172.8	0.65
<i>cdhA</i>	Acetyl-CoA decarboxylase/synthase complex alpha	SBU_001568	1518	70.5	0.05
<i>cdhB</i>	Acetyl-CoA decarboxylase/synthase complex epsilon	SBU_000890	557	120.8	0.64
<i>cdhB</i>	Acetyl-CoA decarboxylase/synthase complex epsilon	SBU_001569	325	65.1	0.35
<i>cdhC</i>	Acetyl-CoA decarboxylase/synthase complex beta	SBU_000889	4798	350.2	0.96
<i>cdhC</i>	Acetyl-CoA decarboxylase/synthase complex beta	SBU_001570	2738	212.9	0.09
<i>cdhD</i>	Acetyl-CoA decarboxylase/synthase complex delta	SBU_000887	3183	232.8	3.03
<i>cdhD</i>	Acetyl-CoA decarboxylase/synthase complex delta	SBU_001572	940	79.6	1.41
<i>cdhE</i>	Acetyl-CoA decarboxylase/synthase complex gamma	SBU_000886	3419	266.4	0.52
<i>cdhE</i>	Acetyl-CoA decarboxylase/synthase complex gamma	SBU_001573	1503	118.6	1.21
<i>metV</i>	5,10-Methylenetetrahydrofolate reductase, C-terminal	SBU_000428	220	36.2	
<i>metF</i>	5,10-Methylenetetrahydrofolate reductase	SBU_000429	487	59.8	0.01
<i>hdrA</i>	Heterodisulfide reductase subunit A	SBU_000430	1435	80.5	
<i>hdrB</i>	Heterodisulfide reductase	SBU_000431	703	45.3	
<i>hdrC</i>	Heterodisulfide reductase	SBU_000432	1259	81.5	
<i>mvhD</i>	Methyl-viologen-reducing hydrogenase delta subunit	SBU_000433	356	53.9	
<i>hdrA</i>	Heterodisulfide reductase subunit A	SBU_000434	839	47.2	
<i>mvhD</i>	Methyl-viologen-reducing hydrogenase delta subunit	SBU_000435	585	154	
<i>metV</i>	5,10-Methylenetetrahydrofolate reductase, C-terminal	SBU_001330	263	39.4	0.25
<i>metF</i>	5,10-Methylenetetrahydrofolate reductase	SBU_001331	711	83.9	0.20
<i>hdr</i>	Heterodisulfide reductase	SBU_001332	392	16.5	
<i>mvhD</i>	Methyl-viologen-reducing hydrogenase delta subunit	SBU_001333	170	57.4	
<i>mch</i>	N(5)N(10)-MethenylH4MPT cyclohydrolase	SBU_000838	197	22.6	0.10
<i>ptr</i>	FormylMF-H4MPT formyltransferase	SBU_001141	416	51.4	0.10
<i>fwdA</i>	Formylmethanofuran dehydrogenase subunit A	SBU_000443	1215	79.2	0.11
<i>fwdB</i>	Formylmethanofuran dehydrogenase subunit B	SBU_000444	555	47.3	
<i>fwdB</i>	Formylmethanofuran dehydrogenase subunit B	SBU_000048	226	21.4	
<i>fwdC</i>	Formylmethanofuran dehydrogenase subunit C	SBU_000442	567	81.3	0.12
<i>fwdD</i>	Formylmethanofuran dehydrogenase subunit D	SBU_000047	75	20.6	
<i>fwdD</i>	Formylmethanofuran dehydrogenase subunit D	SBU_000445	151	43.8	
<i>fwdE</i>	Formylmethanofuran dehydrogenase subunit E	SBU_000903	23	3.8	
<i>fwdF</i>	Formylmethanofuran dehydrogenase subunit F	SBU_001540	91	8.7	

Expression as absolute read counts and as fragments per kilobase of transcript per million mapped reads (FPKM) is shown, as well as the corresponding protein abundance as emPAI index.

Extended Data Table 5 | Genes encoding proteins related to electron cycling and energy transfer in *Ca. S. butanivorans*

Gene	Feature	Locus_tag	Transcriptome		Proteome
			Absolute reads	FPKM	emPAI
	[Ni-Fe]-Hydrogenase large subunit	SBU_000461	5409	343.7	0.28
	[Ni-Fe]-Hydrogenase small subunit	SBU_000462	1702	196.6	
	Cytochrome c-type protein	SBU_000189	324	73.2	
	Cytochrome c	SBU_000960	1161	125.5	0.17
	Cytochrome C	SBU_001187	184	15.3	
	Cytochrome c	SBU_001594	62	5.0	0.21
	Multiheme cytochrome	SBU_000341	196	25.4	
	Multiheme cytochrome	SBU_000342	148	13.1	
	Multiheme cytochrome	SBU_000614	646	83.2	
	Multiheme cytochrome	SBU_000694	4224	659.7	
	Multiheme cytochrome	SBU_000777	3660	571.6	
	Multiheme cytochrome	SBU_000778	3189	395.7	
	Multiheme cytochrome	SBU_001337	1953	389.1	0.61
<i>hdrA</i>	Heterodisulphide reductase, subunit A*	SBU_000297	646	27.0	0.40
<i>hdrB</i>	Heterodisulphide reductase, subunit B*	SBU_000298	1146	146.1	
<i>hdrC</i>	Heterodisulphide reductase, subunit C*	SBU_000299	503	91.7	0.31
<i>fdhB</i>	Formate dehydrogenase subunit beta	SBU_000300	838	86.2	0.89
<i>mvhD</i>	Methyl-viologen-reducing hydrogenase delta	SBU_000301	205	53.9	0.78
<i>fqoJ</i>	F420H2:quinone oxidoreductase subunit J	SBU_000209	3	0.6	
<i>fqoK</i>	F420H2:quinone oxidoreductase subunit K	SBU_000210	12	4.1	
<i>fqoL</i>	F420H2:quinone oxidoreductase subunit L	SBU_000211	133	9.7	
<i>fqoM</i>	F420H2:quinone oxidoreductase subunit M	SBU_000213	166	10.6	
<i>fqoN</i>	F420H2:quinone oxidoreductase subunit N	SBU_000214	142	12.7	
<i>fqoA</i>	F420H2:quinone oxidoreductase subunit A	SBU_000215	85	26.7	0.26
<i>fqoBCD</i>	F420H2:quinone oxidoreductase subunit	SBU_000216	323	15.5	0.04
<i>fqoH</i>	F420H2:quinone oxidoreductase subunit H	SBU_000217	171	17.3	
<i>fqoI</i>	F420H2:quinone oxidoreductase subunit I	SBU_000218	112	16.9	
<i>fqoF</i>	F420H2:quinone oxidoreductase subunit F	SBU_000219	94	10.0	
<i>nuoH</i>	NADH:quinone oxidoreductase subunit H	SBU_000563	446	47.5	0.18
<i>nuoD</i>	NADH:quinone oxidoreductase subunit D	SBU_000564	458	45.7	0.26
<i>nuoC</i>	NADH:quinone oxidoreductase subunit C	SBU_000565	236	56.8	0.69
<i>nuoB</i>	NADH:quinone oxidoreductase subunit B	SBU_000566	345	34.2	
<i>nuoA</i>	NADH:quinone oxidoreductase subunit A	SBU_000567	30	9.4	
<i>nuoI</i>	NADH:quinone oxidoreductase subunit I	SBU_000874	119	34.2	0.23
<i>nuoJ</i>	NADH:quinone oxidoreductase subunit J	SBU_000875	67	30.4	
<i>nuoK</i>	NADH:quinone oxidoreductase subunit K	SBU_000877	69	24.4	
<i>nuoL</i>	NADH:quinone oxidoreductase subunit L	SBU_000878	950	54.5	
<i>nuoM</i>	NADH:quinone oxidoreductase subunit M	SBU_000879	802	57.6	
<i>nuoN</i>	NADH:quinone oxidoreductase subunit N	SBU_000880	994	74.9	

Expression as absolute read counts and as fragments per kilobase of transcript per million mapped reads (FPKM) is shown, as well as the corresponding protein abundance as emPAI index.

\*Submitted as CoB-CoM heterodisulfide reductases.

Extended Data Table 6 | BLASTP search of proteins involved in butyrate oxidation. Best results according to the E-value are shown

Gene product	Locus tag	Blast annotation	Accession number	Organism	Coverage /Identity	E-value
Acyl-CoA dehydrogenase domain-containing protein	SBU_000172	acyl-CoA dehydrogenase	WP_028324559.1	<i>Desulfatirhabdium butyrativorans</i>	100/66	0.0
Acyl-CoA dehydrogenase	SBU_000399	acyl-CoA dehydrogenase	WP_028321791.1	<i>Desulfatiglans anilini</i>	99/51	6e-175
Acyl-CoA dehydrogenase domain-containing protein	SBU_000724	acyl-CoA dehydrogenase	WP_028319806.1	<i>Desulfatiglans anilini</i>	98/62	8e-175
Acyl-CoA dehydrogenase	SBU_001146	hypothetical protein	WP_036734863.1	<i>Peptococcaceae bacterium SCADC1_2_3</i>	97/58	0.0
Crotonase	SBU_000400	hypothetical protein	WP_029475295.1	<i>Dehalococcoidia bacterium SCGC AB-539-J10</i>	96/69	7e-128
3-Hydroxyacyl-CoA dehydrogenase	SBU_000288	3-hydroxybutyryl-CoA dehydrogenase Hbd	EMS78924.1	<i>Desulfotignum phosphitoxidans</i> DSM 13687	100/65	8e-134
3-Hydroxyacyl-CoA dehydrogenase	SBU_000843	3-hydroxy-2-methylbutyryl-CoA dehydrogenase	WP_007907297.1	<i>Ktedonobacter racemifer</i>	98/61	5e-98
Acetyl-CoA acetyltransferase	SBU_000329	acetyl-CoA acetyltransferase	WP_014407007.1	<i>Methanocella conradii</i>	99/67	0.0
Acetyl-CoA acetyltransferase	SBU_000402	conserved hypothetical protein, thiolase family	CBH39006.1	uncultured archaeon	100/70	0.0
Acetyl-CoA acetyltransferase	SBU_000404	conserved hypothetical protein, thiolase family	CBH39006.1	uncultured archaeon	100/57	6e-159
Acetyl-CoA acetyltransferase	SBU_001291	acetyl-CoA acetyltransferase	WP_010917519.1	<i>Thermoplasma volcanium</i>	98/43	4e-103

Extended Data Table 7 | Genes encoding Type IV pili and 10 most expressed cytochromes identified in the HotSeep-1 genome bin from the Butane50 culture

Gene	Feature	Best Blast Hit		Pfam hits	Transcriptome		
		Accession number	Coverage/Identity	Domain ID/accession	Absolute reads	FPKM	
PilA	type IV pilus assembly protein	AMM41792.1	100/99	N_methyl_3/PF13633.3	8	3	
PilA	pilus assembly protein PilA	AMM39924.1	100/88	N_methyl_3/PF13633.3	1780	582	
Peptidase A24	peptidase A24	AMM42236.1	100/100	Dis_P_Dis/ PF06750; Peptidase_A24/ PF01478	31	9	
PilQ	pilus modification protein PilQ	AMM40410.1	100/99	AMIN/ PF11741; STN/ PF07660; Secretin_N/ PF03958; Secretin/PF00263	116	12	
PilP	type IV pilus assembly protein PilP	AMM40409.1	100/99	T2SSC/ PF11356; PilP/PF04351	8	4	
PilO	pilus assembly protein PilO	AMM40408.1	100/100	PilO/PF04350	7	2	
PilN	type IV pilus assembly protein PilN	AMM40407.1	100/98	PilN/PF05137	13	5	
PilM	pilus assembly protein PilM	AMM40406.1	100/99	Pil_2/PF11104	32	6	
PilW	putative pilus assembly protein PilW	AMM39834.1	100/99	N_methyl_2/PF13544	53	10	
PilY1	type IV pilus assembly protein	AMM41700.1	100/98	-	247	12	
PilY1	putative pilus assembly protein PilY	AMM41699.1	100/99	Neisseria_PilC/PF0556 7	91	16	
PilL	type IV pilus assembly protein pilL	AMM41701.1	100/93	-	3	2	
PilC	type IV pilus assembly protein PilC	AMM42043.1	97/99	T2SSF/PF00482 (x2)	50	9	
Cytochrome c type based on PfamA domain prediction	Feature	Best Blast Hit		Cellular localization (PSORTb) <sup>1</sup>	Heme groups	Transcriptome	
		Accession number	Coverage/identity			Absolute reads	FPKM
Cytochrom_CIII	class III cytochrome C	AMM42051.1	100/97	Periplasmic	4	505	238
Paired_CXXCH_1	doubled CXXCH cytochrome C	AMM40456.1	99/46	Extracellular	5	1244	232
Paired_CXXCH_1	doubled CXXCH cytochrome C	AMM40456.1	100/94	Unknown (CM,P,OM,E)	6	768	143
Paired_CXXCH_1	doubled CXXCH cytochrome C	AMM39976.1	100/94	Unknown (CM,P,OM,E)	7	471	94
Paired_CXXCH_1	cytochrome C	AMM40455.1	96/95	Extracellular	6	483	96
Cytochrom_CIII	class III cytochrome C	AMM41048.1	100/99	Periplasmic	4	69	31
Paired_CXXCH_1	cytochrome C	AMM40346.1	100/99	Cytoplasmic	10	135	28
Paired_CXXCH_1	cytochrome C	AMM40455.1	99/46	Periplasmic	7	105	21
Cytochrom_c3_2	cytochrome C	AMM40350.1	100/100	Unknown (CM,P,E)	12	72	17
Cytochrom_c3_2	cytochrome C	AMM40349.1	100/99	Periplasmic	12	53	14

<sup>1</sup>For unknown cellular localization of cytochromes, potential locations are indicated according to the score value; CM, cytoplasmic membrane; P, periplasmic; OM, outer membrane; E, extracellular.